HHS Public Access

Author manuscript

*Immunity*. Author manuscript; available in PMC 2024 April 11.

Published in final edited form as:

*Immunity*. 2023 April 11; 56(4): 768–782.e9. doi:10.1016/j.immuni.2023.01.027.

# Non-canonical pattern recognition of a pathogen-derived metabolite by a nuclear hormone receptor identifies virulent bacteria in *C. elegans*

**Nicholas D. Peterson**[1,3], **Samantha Y. Tse**[1,3], **Qiuyu Judy Huang**[2], **Khursheed A. Wani**[1], **Celia A. Schiffer**[2], **Read Pukkila-Worley**[1,4,*]

[1]Program in Innate Immunity, Division of Infectious Diseases and Immunology, Department of Medicine, University of Massachusetts Chan Medical School, Worcester, MA 01655, United States of America,

[2]Department of Biochemistry and Molecular Biotechnology, University of Massachusetts Chan Medical School, Worcester, MA 01655, United States of America,

[3]These authors contributed equally to this work,

[4]Lead contact

## SUMMARY

Distinguishing infectious pathogens from harmless microorganisms is essential for animal health. The mechanisms used to identify infectious microbes are not fully understood, particularly in metazoan hosts that eat bacteria as their food source. Here, we characterized a non-canonical pattern recognition system in *Caenorhabditis elegans* that assesses the relative threat of virulent *P. aeruginosa* to activate innate immunity. We discovered that the innate immune response in *C. elegans* was triggered by phenazine-1-carboxamide (PCN), a toxic metabolite produced by pathogenic strains of *Pseudomonas aeruginosa*. We identified nuclear hormone receptor NHR-86/HNF4 as the PCN sensor in *C. elegans* and validated that PCN bound to the ligand-binding domain of NHR-86/HNF4. Activation of NHR-86/HNF4 by PCN directly engaged a transcriptional program in intestinal epithelial cells that protected against *P. aeruginosa*. Thus, a bacterial metabolite is a pattern of pathogenesis surveilled by nematodes to identify a pathogen among its bacterial diet.

## Graphical Abstract

*Correspondence may be addressed to Read Pukkila-Worley (Read.Pukkila-Worley@umassmed.edu, @RPWlab).

Author contributions:

Conceptualization: NDP, SYT, RPW; Methodology: NDP, SYT, QJY, CAS, RPW; Investigation: NDP, SYT, QJY, KAW; Visualization: NDP, SYT, QJY; Funding acquisition: RPW; Project administration: RPW; Supervision: RPW; Writing – original draft, NDP, SYT, RPW; Writing – review & editing, NDP, SYT, QJY, CAS, RPW



Competing interests:

Authors declare that they have no competing interests.

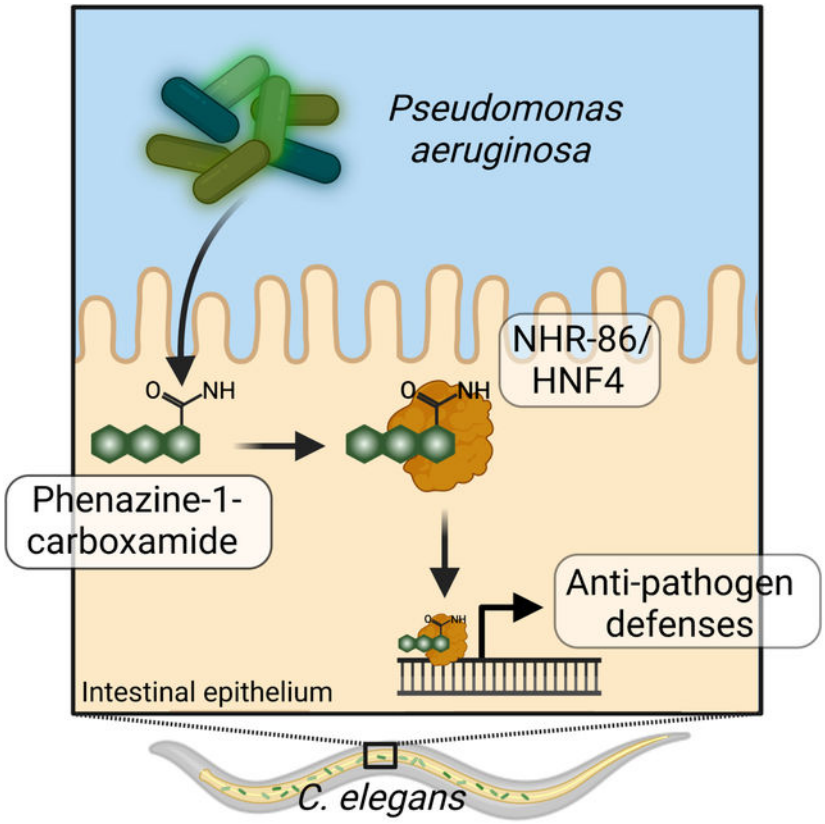


## eTOC blurb

Immune sensing of infectious microorganisms is essential for animal health. Peterson and Tse, et al. characterize a non-canonical pattern recognition system that intercepts pathogen-derived signals of growth and virulence to assesses the relative threat of virulent bacteria. A *Caenorhabditis elegans* nuclear hormone receptor senses phenazine-1-carboxamide (PCN), a toxic metabolite produced by pathogenic strains of *Pseudomonas aeruginosa*, to activate innate immunity.

### Keywords

Pattern recognition receptor; nuclear hormone receptor; phenazines; *Pseudomonas aeruginosa* ; *Caenorhabditis elegans*

## INTRODUCTION

The ability to discriminate pathogens from beneficial microorganisms is essential for the health of all metazoan animals. This problem is particularly challenging for organisms, such as free-living nematodes, that eat bacteria as their food source and are thus constantly exposed to bacterial features that activate immune defenses in other metazoans [*i.e.*, microbe- or pathogen-associated molecular patterns (MAMPs/PAMPs)][1]. Indeed, nematodes lost classical mechanisms of pattern recognition for the detection of pathogens during evolution[2,3]. *Caenorhabditis elegans*, for example, does not utilize pattern recognition

receptors, such as members of the Toll-like receptor (TLR) or nucleotide-binding and oligomerization domain (NOD)-like receptor (NLR) protein families, to detect microbial infection and yet are still able to mount pathogen-specific immune defenses[4–6].

The innate immune response in *C. elegans* requires the function of conserved signaling regulators, such as the p38 PMK-1 immune pathway, that maintain the constitutive or tonic expression of immune effector genes[7,8]. Dietary cues, inputs from sensory neurons, and changes in the availability of essential host metabolites, such as cholesterol, adjust the basal activity of the p38 PMK-1 pathway to prime immune effector expression during periods of relative vulnerability to infection[8–14]. *C. elegans* also evolved mechanisms to sense pathogens indirectly to target host defenses toward invading pathogens or secreted toxins. For example, the G protein-coupled receptor DCAR-1 in the *C. elegans* hypodermis recognizes a host ligand, or damage-associated molecular pattern, that is elaborated as a sequela of fungal infection[15]. *C. elegans* also activates immune defenses in response to perturbations in host physiology that accompany infection with pathogenic microbes or the effects of their secreted toxins, a process that is often called surveillance immunity[16–20]. In addition, bloating of the *C. elegans* intestinal lumen induced by microbial colonization activates a behavioral avoidance response and the transcription of immune effector genes[21–23]. However, whether *C. elegans* has evolved mechanisms for direct detection of pathogens, akin to the classical mechanisms of pattern recognition present in other metazoan animals, remains unknown.

Bacteria produce a wide array of metabolites that regulate growth, virulence, and intra- and inter-species interactions[24,25]. Thus, these molecules may readout the virulence potential of pathogens and be intercepted by hosts to program adaptive defenses. Phenazine metabolites produced by *Pseudomonas aeruginosa*, for example, are sensed by chemosensory neurons in *C. elegans*, which activates the transcription of a TGF-β family member *daf-7*. Neuroendocrine signaling controlled by DAF-7 is necessary for *C. elegans* to induce protective avoidance behavior in the presence of *P. aeruginosa*[26]. However, individual phenazines produced by *P. aeruginosa* do not elicit *C. elegans* avoidance behavior, and wild-type nematodes still readily avoid pseudomonal mutants that are unable to make phenazines[21]. Thus, the behavioral responses of *C. elegans* to *P. aeruginosa* in this context are likely multi-factorial.

Nuclear hormone receptors are a large family of transcription factors that are regulated by small molecule ligand binding. Compared to other metazoans, *C. elegans* express an expanded family of nuclear hormone receptors compared to other metazoans – 274 are present in *C. elegans*, whereas *Drosophila* and humans have only 21 and 48, respectively[27–30]. The marked expansion of this protein family suggests that these transcription factors have important roles in nematode physiology, potentially as direct sensors of bacterial metabolites. However, very few *C. elegans* nuclear hormone receptors have been characterized in detail and the ligands for only four have been determined, none of which are produced by bacteria[31–36].

Here, we demonstrated that a *C. elegans* nuclear hormone receptor, which is a homolog of mammalian HNF4, is a bacterial pattern recognition receptor that senses a pathogen-derived

metabolite to activate anti-pathogen defenses. We discovered that phenazine-1-carboxamide (PCN), a toxic phenazine metabolite produced by *P. aeruginosa*, bound to and activated the *C. elegans* nuclear hormone receptor NHR-86/HNF4. We showed that activated NHR-86/HNF4 trafficked to the promoters of infection-response genes, independent of intermediary signaling pathways, to engage a transcriptional program that provided protection from bacterial killing. We also showed that PCN specifically marked *P. aeruginosa* in a disease-causing state. Thus, PCN is a pattern of pathogenesis[37] sensed by *C. elegans*, rather than canonical MAMPs, to identify an infectious bacterial pathogen from among its bacterial food and to activate innate immunity.

## RESULTS

### The pathogen-derived metabolite phenazine-1-carboxamide (PCN) activates anti-pathogen defenses in the *C. elegans* intestine.

To determine how *C. elegans* senses infection by the bacterial pathogen *P. aeruginosa*, we examined *P. aeruginosa* strains with mutations in key transcriptional regulators that control pathogen virulence (Fig. 1A, Fig. S1A–C)[38]. For these studies, a transgenic *C. elegans* strain that carries a GFP-based transcriptional reporter for infection response gene (*irg*)-4, a secreted immune effector that is transcriptionally induced in the intestine during bacterial infection, was used as an *in vivo* sensor of immune activation[7,9,39–44]. Mutations in three of the 17 *P. aeruginosa* transcriptional regulators eliminated the induction of *C. elegans irg-4*p::*gfp* during infection: pseudomonal mutants in *rhlR*, *pqsR*, and *lasR* (Fig. 1A, Fig. S1A–C). *P. aeruginosa* RhlR, PqsR, and LasR are each transcription factors that function in bacterial quorum-sensing pathways and together control the expression of so-called group behavior genes, which include virulence effectors[45,46]. Thus, we undertook a secondary screen of 152 *P. aeruginosa* strains with mutations in genes known to be regulated by one of these transcription factors, RhlR[47], to identify individual pseudomonal effectors that drive *C. elegans* immune activation (Fig. S1D). We identified only three hits in this screen (*phzA2*, *phzB2*, and *phzH*), all of which contained mutations in phenazine biosynthesis genes[48] (Fig. S1E). *C. elegans irg-4*p::*gfp* immune reporter animals infected with a *P. aeruginosa* strain containing clean deletions in both phenazine biosynthesis operons [*P. aeruginosa* Δ*phz* mutant[49]] failed to upregulate *irg-4*p::*gfp* in the intestine during infection (Fig. 1A). RNA-sequencing confirmed that *P. aeruginosa* phenazine biosynthesis is required for *C. elegans* innate immune activation (Fig. 1B). Importantly, this experiment identified a group of *C. elegans* genes whose induction during *P. aeruginosa* infection was entirely dependent on the production of phenazines (Fig. 1B). Of these 27 genes, 22 are *C. elegans* innate immune effectors or detoxification genes (Fig. 1B, Table S1A). Examination of transcriptional reporters for the anti-pathogen gene *irg-5* (Fig. S1F) and the cytochrome p450 gene *cyp-35C1* (Fig. S1G) confirmed that the induction of these genes in the intestine was abrogated during infection with the *P. aeruginosa* Δ*phz* mutant.

*P. aeruginosa* produces four major phenazine metabolites: phenazine-1-carboxylic acid (PCA), phenazine-1-carboxamide (PCN), pyocyanin (PYO), and 1-hydroxyphenazine (1-HP) (Fig. 1C)[48]. Importantly, supplementation with PCN, but not the three other secreted phenazine metabolites, was sufficient to restore both *C. elegans irg-4*p::*gfp* (Fig. 1D) and

*cyp-35C1*p::*gfp* (Fig. S1H) activation in the *P. aeruginosa* Δ*phz* mutant. Additionally, in the absence of infection, supplementing PCN, but not the three other phenazines, drove the dose-dependent activation of *C. elegans irg-4*p::*gfp* (Fig. 1E, Fig. S1I) and *cyp-35C1*p::*gfp* expression (Fig. S1J); a finding that was confirmed by qRT-PCR analysis for these and other innate immune effectors (Fig. 1F).

Consistent with the role of PCN in inducing *C. elegans* innate immune defenses, infection with a *P. aeruginosa* strain containing a mutation in *phzH*, a glutamine amidotransferase that synthesizes PCN (Fig. 1C), abrogated the induction of *C. elegans irg-4*p::*gfp* (Fig. 1G), *irg-5*p::*gfp* (Fig. S1K), and *cyp-35C1*p::*gfp* expression (Fig. S1L). We used liquid chromatography-mass spectrometry (LC-MS/MS) to confirm that the *P. aeruginosa phzH* mutant is deficient in the production of PCN but not the other phenazine molecules (Fig. S1M). Notably, *C. elegans* infected with *P. aeruginosa* strains with mutations in either *phzM* or *phzS*, the enzymes that synthesize PYO and 1-HP (Fig. 1C), did not affect the induction of these immune effectors (Fig. 1G, Fig. S1K and L). Moreover, we found that the transcriptional signature of *C. elegans* exposed to PCN mimics that of animals infected with *P. aeruginosa* (Fig. 1H, Table S1B). Thus, the *P. aeruginosa* metabolite PCN specifically and robustly activates *C. elegans* intestinal innate immune defenses.

## The anti-pathogen transcriptional program induced by PCN requires the *C. elegans* nuclear hormone receptor *nhr-86*.

To identify the *C. elegans* receptor for PCN, we focused our analysis on nuclear hormone receptors given their function as ligand-gated transcription factors that can potentially sense bacterial metabolites. We used RNAi to screen 271 of 274 nuclear hormone receptor genes in the *C. elegans* genome and identified one hit that strongly suppressed *C. elegans irg-4*p::*gfp* immune reporter induction by PCN: *nhr-86* (Fig. S2A). Knockdown of *nhr-86* abrogated the induction of *C. elegans irg-4*p::*gfp* (Fig. 2A) and *cyp-35C1*p::*gfp* (Fig. 2B) by PCN treatment and during *P. aeruginosa* infection. Two *nhr-86* loss-of-function alleles *tm2590*[50] and *ums12*[39] fully suppressed the induction of *irg-4*p::*gfp* (Fig. 2C) and *irg-5*p::*gfp* (Fig. S2B) under these conditions. We used CRISPR-Cas9 to tag *nhr-86* with an auxin-inducible degron (AID) at its endogenous locus. Treatment with the phytohormone auxin in a transgenic *C. elegans* strain expressing the auxin-binding receptor transport inhibitor response 1 (TIR1) targets NHR-86::AID for degradation by the proteasome in all tissues[51]. We confirmed that auxin treatment induced the degradation of NHR-86::AID protein in this strain (Fig. S2C). Depletion of NHR-86 abrogated the induction of *irg-4* following exposure to PCN (Fig. 2D) and during *P. aeruginosa* infection (Fig. 2H), findings that are consistent with our prior study[39]. We also found that the PCN- and *P. aeruginosa*-mediated induction of *irg-5* (Figs. 2E and 2I), *cyp-35C1* (Figs. 2F and 2J) and *ugt-13* (Figs. 2G and 2K) was attenuated in NHR-86-depleted animals. Consistent with these data, RNA-sequencing revealed that *nhr-86* is required for the induction of *C. elegans* genes following exposure to PCN (Fig. 2L, Fig. S2D, Table S1C). In this experiment, the transcriptomes of wild-type and *nhr-86(RNAi) C. elegans* animals, each exposed to solvent control or PCN, were compared. These data revealed that 63 of the 133 genes upregulated by PCN in wild-type worms ($q<0.05$) required *nhr-86* for their induction (Fig. 2L, Fig. S2D, Table S1C).

We performed chromatin immunoprecipitation to characterize the promoter occupancy of NHR-86 at baseline and during PCN treatment using GFP-tagged NHR-86 protein (NHR-86::GFP) and an anti-GFP antibody. NHR-86 was enriched at the promoters of the four representative anti-pathogen effector genes during PCN treatment, but not in untreated controls (Fig. 2M–P). Importantly, there was no enrichment of NHR-86 at these promoter regions in wild-type animals (which do not express NHR-86::GFP) that were exposed to PCN (Fig. 2M–P). Furthermore, PCN exposure did not cause enrichment of NHR-86 at two intergenic regions in chromosome IV (Fig. 2Q and R). The p38 MAP kinase PMK-1 pathway is a central regulator of anti-pathogen defenses in *C. elegans* that controls the basal expression of immune effector genes, including *irg-4* and *irg-5*. Consistent with our NHR-86 promoter occupancy data, we found that PCN did not induce the phosphorylation of the p38 MAP kinase PMK-1, as measured in a Western blot experiment using antibodies that specifically recognize the doubly phosphorylated TGY motif of activated PMK-1 and the total PMK-1 protein (Fig. S2E and F). Together, these data demonstrate that PCN causes NHR-86 to traffic directly to the promoters of innate immune effector genes to activate their transcription, independent of the p38 PMK-1 pathway.

In a previous study, we showed that NHR-86 activates the transcription of intestinal immune defense genes in the presence of a synthetic immunostimulatory molecule (R24)[39]. Indeed, we found that, upon activation by R24, NHR-86 traffics to the promoters of immune effectors that we also identified as NHR-86 targets following PCN treatment[39]. Consistent with these findings, PCN and R24 induced similar transcriptional signatures (Fig. S2G, Table S1D). Furthermore, the *nhr-86*-dependent genes that were induced during PCN treatment and those that were upregulated by *nhr-86* following R24 treatment were also tightly correlated (Fig. S2H, Table S1E). These data suggest that the bacterial metabolite PCN and the xenobiotic R24 each activate NHR-86 to induce anti-pathogen defenses.

NHR-86 principally localizes to the nuclei of intestinal epithelial cells and several neurons[50]. NHR-86 directly regulates the transcription of innate immune effector genes, such as *irg-4*, *irg-5* and *cyp-35C1*, that are expressed in intestinal epithelial cells (Figs. 1 and 2). Consistent with this observation, knockdown of *nhr-86* only in intestinal epithelial cells, using a transgenic *C. elegans* strain engineered to perform RNAi only in this tissue, suppressed the induction of *irg-4* by PCN (Fig. S2I). These data suggest that NHR-86 functions in intestinal epithelial cells to activate the transcription of anti-pathogen defenses.

Chemosensation of *P. aeruginosa* secondary metabolites, including PCN, induces the transcription of the TGF-β family member *daf-7* in ASJ chemosensory neurons[26]. While *daf-7* is required for *C. elegans* to avoid *P. aeruginosa*[26], individual phenazines, including PCN, do not induce avoidance behavior in *C. elegans*[21]. In addition, wild-type nematodes still readily avoid *P. aeruginosa* with mutations in the genes that make phenazines, including *phzH* mutants[21]. Importantly, the induction of *C. elegans irg-4*p::*gfp* by PCN occurs independently of *daf-7* (Fig. S2J). In addition, auxin-induced degradation of *C. elegans* NHR-86::AID does not alter the avoidance response to *P. aeruginosa* (Fig S2K). Together, these data indicate that *C. elegans* behavioral responses to *P. aeruginosa* occur independently of PCN sensing by NHR-86.

Individual phenazines produced by *P. aeruginosa* also activate the mitochondrial unfolded protein response ($UPR^{mt}$) in a manner that requires the transcription factor ATFS-1[52,53]. However, knockdown of *atfs-1* by RNAi did not suppress *irg-4*p::*gfp* induction during *P. aeruginosa* infection (Fig. S2L). Additionally, induction of mitochondrial stress by either treatment with mitochondrial poisons (Fig. S2M) or knockdown of a key mitochondrial protease, *spg-7* (Fig. S2N), did not lead to *irg-4*p::*gfp* induction. Likewise, gene set enrichment analysis of genes differentially expressed in wild-type animals following treatment with PCN did not reveal a signature of a mitochondrial stress response induced by either *spg-7(RNAi)* (Fig. S2O) or in the *atfs-1(et18)* gain-of-function mutant (Fig. S2P). Collectively, these data demonstrate that the activation of innate immune defenses by PCN occurs through *nhr-86* and not via previously characterized responses to *P. aeruginosa* phenazines.

## The bacterial metabolite PCN and synthetic immunostimulatory molecule R24 bind to the ligand-binding domain of NHR-86.

To determine if PCN and R24 are ligands of NHR-86, we performed biophysical assays. We expressed and purified the ligand-binding domain (LBD) of NHR-86 from *E. coli* (Fig. S3A) and measured the intrinsic tryptophan fluorescence in the presence of R24 and PCN. Ligand binding to its target protein quenches the fluorescence of tryptophan residues in the protein[54]. PCN (Fig. 3A) and R24 (Fig. 3B) each decreased the intrinsic tryptophan fluorescence intensity of the NHR-86(LBD) in a dose-dependent manner. The equilibrium dissociation constants ($K_d$), which characterizes the affinity of PCN and R24 for the NHR-86(LBD), are 24.24 μM and 5.53 μM, respectively (Fig. 3A and B). Importantly, PCA, which does not activate host innate immune defenses (Fig. 1D and E, Fig. S1H and J), did not suppress the intrinsic tryptophan fluorescence of the NHR-86(LBD) (Fig. 3A).

As an orthologous means to demonstrate that PCN and R24 bind to NHR-86, we utilized a cellular thermal shift assay (CETSA), a technique based on the principle that the binding of a ligand to its target stabilizes the protein complex against denaturing and aggregating at higher temperatures[55]. For these studies, we used CRISPR-Cas9 to insert a 3xFLAG tag at the N-terminus of the NHR-86 protein. As a control, we used a strain expressing a transgene that contains a 3xFLAG-labeled NHR-12 protein[56], which is the closest nematode paralog of NHR-86[30]. Using these strains, we probed for either NHR-86 or NHR-12 in whole-cell lysates using an anti-FLAG antibody. PCN and R24 treatments each led to thermal stabilization of NHR-86 over a range of temperatures (Fig. 3C–E, Fig. S3B). We quantified the area under the curve from biological replicates and found that treatment with PCN and R24 each increased the thermal stability of NHR-86 (Fig. 3E, Fig. S3B). The thermal stabilization of NHR-86 by PCN was reproducible, significant, and more subtle than by R24. Importantly, R24 and PCN each failed to thermally stabilize NHR-12 (Fig. 3F and G, Fig. S3C). In addition, the phenazine metabolite PCA, which does not activate host innate immune defenses (Fig. 1D and E, Fig. S1H and J), did not thermally stabilize NHR-86 (Fig. 3C–E, Fig. S3B).

To further characterize the binding of R24 and PCN to NHR-86, we modeled the three-dimensional structure of the protein *in silico* (Fig. 4A). HNF4α, the mammalian homolog

of *C. elegans* NHR-86, forms a stable homodimer[57], and thus, we used this conformation to model NHR-86. We docked PCN, R24, and PCA into a potential ligand-binding pocket identified in the NHR-86(LBD) (Fig. 4A) and used molecular dynamics simulations to calculate the free energy of binding for these molecules. We found that R24 and PCN each bind stably to NHR-86(LBD), whereas PCA does not (Fig. 4B, Supplemental Video S1). These calculations also predicted that R24 has an increased affinity for the NHR-86(LBD) compared to PCN, a finding that was confirmed experimentally in both the intrinsic tryptophan fluorescence quenching biophysical assays (Fig. 3A and B) and the CETSA thermal stabilization (Fig. 3C–E). Consistent with these data, R24 causes a more robust induction of anti-pathogen effector genes than PCN at equimolar concentrations (Fig. 4C–F).

Examination of both PCN and R24 docked *in silico* within the binding pocket of NHR-86(LBD) revealed that the phenylalanine (F) at residue 379 interacts with each of these ligands (Fig. 4G, Fig. S4A). We used CRISPR genome editing to mutate this amino acid (F379H) in *C. elegans* animals. Importantly, PCN and R24 were not able to thermally stabilize 3xFLAG::NHR-86$^{F379H}$ in CETSA experiments performed as described above (Fig. 4H–J, Fig. S4B). Additionally, we expressed and purified from *E. coli* the NHR-86(LBD)$^{F379H}$ mutant protein (Fig. S3A). The NHR-86(LBD)$^{F379H}$ mutation attenuated the quenching of the intrinsic tryptophan fluorescence by both PCN and R24 (Fig. 4K) compared to the wild-type NHR-86(LBD) protein. Thus, F379 in NHR-86 is required for the binding of PCN and R24 to the ligand-binding domain of NHR-86. Importantly, we introduced the *C. elegans nhr-86*$^{F379H}$ mutation into the genome using CRISPR-Cas9 and found that immune effector induction following PCN treatment was attenuated in these mutants (Fig. 4L–P). We introduced a 3xFLAG to tag the NHR-86$^{F379H}$ protein in this strain and confirmed that it was translated at wild-type levels (Fig. S4C).

In summary, these data demonstrate that PCN directly binds to the ligand binding domain of NHR-86.

## The bacterial metabolite PCN is a pattern of pathogenesis sensed by *C. elegans* NHR-86 to activate innate immunity.

Phenazine metabolites rapidly kill *C. elegans* in a model of acute pathogen toxicity (also called the “fast kill” assay) and are required for the full virulence potential of *P. aeruginosa* in mice[58–60]. As previously observed, phenazine toxins secreted into the agar by *P. aeruginosa* rapidly killed wild-type *C. elegans* (Fig. 5A and B, Fig. S5)[58,59]. Exposure to exogenous PCN protected *C. elegans* from phenazine-mediated killing in this assay (Fig. 5A and B), data that agree with our hypothesis that *C. elegans* uses PCN as a recognition signal to protect itself from intoxication by *P. aeruginosa*. Furthermore, post-embryonic degradation of *C. elegans* NHR-86::AID protein abrogated the protection conferred by PCN against phenazine-mediated killing (Fig. 5A and B).

Using a pathogenesis assay that examines intestinal infection by *P. aeruginosa* (the “slow kill” assay)[61], we previously observed that the synthetic immunostimulatory small molecule R24 provided protection from infection of *C. elegans* by *P. aeruginosa* in a manner dependent on *nhr-86*[39]. Consistent with these data and the observation that PCN activates

the transcription of infection response genes, such as *irg-4* (Fig. 2D) and *irg-5* (Fig. 2E), PCN treatment also extends the lifespan of *C. elegans* infected with *P. aeruginosa* (Fig. S5B). *nhr-86(RNAi)* abrogated the protection from *P. aeruginosa* killing conferred by PCN treatment. Of note, the PCN-mediated lifespan extension during *P. aeruginosa* infection was more subtle than that conferred by R24 treatment (Table S2)[39]. These data are consistent with the observation that R24 binds more tightly to the binding pocket of NHR-86 (Fig. 3) and more potently activates the transcription of anti-pathogen effectors (Figs. 4C–F) than PCN.

We assessed the toxic effects of PCN itself (*i.e.*, in the absence of pathogen) by examining the development of *C. elegans* in the presence or absence of this phenazine (Fig. 5C and D). PCN was mildly toxic to wild-type worms. However, PCN treatment was deleterious to the growth and survival of *C. elegans* with degraded NHR-86::AID protein (Fig. 5C and D). Thus, NHR-86 mobilizes a host response that counteracts the toxicity of PCN. We conclude that the toxic bacterial metabolite PCN is a pattern of pathogenesis sensed by *C. elegans* NHR-86 to activate protective anti-pathogen defenses.

### *C. elegans* sense PCN to assess the relative threat of virulent *P. aeruginosa*, but not other pathogenic bacteria.

In its natural habitat, *C. elegans* encounter *Pseudomonas* sp. that likely encode the phenazine biosynthetic operon[62,63]. We therefore hypothesized that *C. elegans* senses PCN to assess the relative threat of virulent *P. aeruginosa* in its environment. We found that the amount of PCN, as quantified by liquid chromatography, in strains of *P. aeruginosa* with varying degrees of virulence potential (PA14, PAO1, and PAK) correlated with the production of the other toxic phenazines in these strains [PCA (Fig. 6A), 1-HP (Fig. S6A), and PYO (Fig. S6B)]. These data are noteworthy considering that NHR-86 senses only PCN and not PCA (Figs. 3 and 4) or the other phenazines (Fig. 1D and E) to activate anti-pathogen defenses. Accordingly, the *P. aeruginosa* strains that produced more PCN had enhanced pathogenicity (Fig. 6B) and more robustly induced the *C. elegans* anti-pathogen effectors *irg-4*p::*gfp*[41] and *cyp-35C1*p::*gfp* (Fig. S6C).

We drove phenazine production in *P. aeruginosa* PAO1, a strain that naturally produces fewer phenazines (Fig. 6A) and is less pathogenic than PA14 (Fig. 6B), by overexpressing *pqsE*, a pseudomonal gene necessary for phenazine production by the *rhl* quorum-sensing pathway[64–66]. Overexpressing *pqsE* in *P. aeruginosa* PAO1, and also in PA14, increased phenazine production, including PCN and PCA (Fig. 6C and D, Fig. S6D and E), enhanced the induction of *C. elegans irg-4*p::*gfp* (Fig. 6E), and augmented the pathogenicity of these strains (Fig. 6F and G). Furthermore, the quantity of PCN produced in these *P. aeruginosa* overexpression strains directly correlated with their virulence potential toward *C. elegans* (Fig. 6H). These data establish a direct connection between phenazine production in *P. aeruginosa*, pathogen virulence potential, and the activation of anti-pathogen defenses in nematodes.

The transcriptional signature of *C. elegans* exposed to PCN specifically marks infection with *P. aeruginosa*, but not other bacterial pathogens (Fig. 6I–L). We compared the *C. elegans* genes induced during infection with five gram-negative (*P. aeruginosa, Serratia*

*marcescens, Photorhabdus luminescens, Erwinia carotovora*, and *Shigella flexneri*) and two gram-positive (*Enterococcus faecalis* and *Staphylococcus aureus*) bacterial pathogens with those that are differentially expressed following exposure to PCN. Only the genes that are upregulated during *P. aeruginosa* infection were enriched in this comparison (Fig. 6I and J). In addition, we observed significant overlap with the genes that require *nhr-86* for their proper expression and the genes that are upregulated during *P. aeruginosa* infection, but not the six other pathogens (Fig. 6K and L). Thus, we conclude that *C. elegans* sense PCN specifically to assess the relative threat of virulent *P. aeruginosa*, but not other pathogenic bacteria.

## DISCUSSION

Although it is well-established that *C. elegans* coordinates inducible immune defenses to provide protection during pathogen infection, the identification of immune receptors that are directly involved in pathogen recognition in nematodes has been elusive. Here, we demonstrated that a *C. elegans* nuclear hormone receptor is a *bona fide* pattern recognition receptor that detects the pathogen-derived metabolite PCN. We showed that PCN bound to the ligand-binding domain of NHR-86, which then directly activated anti-pathogen defenses that provided protection from *P. aeruginosa*. In addition, we found that PCN is sensed in *C. elegans* to assess the relative threat of virulent *P. aeruginosa* specifically, but not other pathogenic bacteria. Thus, we conclude that PCN is a pattern of pathogenesis[37] sensed by *C. elegans* to detect an individual bacterial pathogen in a specific manner from among its bacterial food.

Pattern recognition of pathogen-derived metabolites is a distinct model of immune sensing in the bacteriovore *C. elegans*, an organism that does not use canonical pattern recognition receptors, such as Toll-like receptors, to activate innate immunity. We speculate that *C. elegans* lost canonical MAMP/PAMP-driven mechanisms of pattern recognition because these microbial elements are ubiquitous in the natural habitat of nematodes and thus, are insufficient to distinguish disease-causing pathogens from microbial food sources. Sensing of pathogen-specific metabolic signatures by host nuclear hormone receptors is reminiscent of the immune response in plants, in which specific host-encoded resistance (R) proteins evolved to sense individual pathogen-derived virulence determinants (so-called R gene-effector pairs)[67,68]. *C. elegans* encode 274 nuclear hormone receptors. Thus, decoding the metabolic signatures of bacterial pathogens by these ligand-activated transcription factors is an evolutionarily adaptable mechanism that allows nematodes to distinguish a broad range of pathogens from nonpathogenic bacterial food. Further studies are needed to identify additional nuclear hormone receptor / pattern of pathogenesis pairs.

Bacteria are the only known natural producers of phenazine metabolites[69]. In addition to *Pseudomonas* sp., diverse environmental bacteria, such as *Burkholderia* sp., *Streptomyces* sp., and *Nocardia* sp., encode the phenazine biosynthetic operon and synthesize these molecules[48,70–72]. In *P. aeruginosa*, the production of phenazines is controlled by quorum-sensing pathways that are activated when bacteria reach high cellular density, such as during growth in biofilms[58,60,71]. These molecules contribute to pseudomonal pathogenesis during infection, likely by interrupting electron transport in mitochondria[53,58]. In addition,

phenazines (PCN, in particular) are predominant in *P. aeruginosa* biofilms where they help to maintain redox balance within the relatively anoxic environment of the biofilm interior[25,60]. The *phzH* gene, which encodes the enzyme that synthesizes PCN, is not located in the phenazine biosynthetic operon and may be exclusively expressed in *Pseudomonas* sp.[48,70]. Thus, PCN production may be specifically associated with *P. aeruginosa* that are in a disease-causing growth state and mark strains that elaborate toxic phenazines – one aspect of virulence in a bacterial species with multiple mechanisms of pathogenesis[73].

Multiple transcriptional regulators control the expression of overlapping sets of immune effectors in *C. elegans*. For example, the transcription factor ATF-7 functions downstream of the p38 PMK-1 immune pathway to control the basal, or resting, expression of innate immune genes[74]. During *P. aeruginosa* infection or PCN exposure, many of these immune genes are induced by NHR-86 in a manner independent of p38 PMK-1/ATF-7 signaling. Our group and others have shown that the basal activity of the p38 PMK-1 pathway is adjusted in response to micronutrient scarcity, changing environmental conditions and inputs from chemosensory neurons[8–14]. We have proposed that immune effector priming in this manner is a mechanism to anticipate threats during periods of relative vulnerability to pathogen infection[8]. In this context, bacterial patterns of pathogenesis are sensed by nuclear hormone receptors to further augment immune effector expression in a manner that provides pathogen- or pathogen effector-specific protection.

Importantly, phenazines also activate innate immunity in mammals through interaction with the aryl hydrocarbon receptor (AhR), a protein that recognizes a diverse array of ligands, including environmental toxins and endogenous ligands[75,76]. Thus, the interpretation of bacterial metabolites as a mechanism to direct host defenses towards potential pathogens may be among the most primordial forms of immune sensing in all metazoans.

## Limitations of the study

Sensing of the pathogen-derived phenazine metabolite PCN by NHR-86 activated protective host defenses that enabled *C. elegans* to survive challenge with *P. aeruginosa*. In addition, we found that *C. elegans* with depleted *nhr-86* protein were not more susceptible to phenazine-mediated pathogenesis in the “fast kill” assay, findings that are consistent with our prior report[39]. There are several possible explanations that could account for the observed lack of a pathogen-susceptibility phenotype in *nhr-86*-depleted animals. The amount of PCN produced by pathogenic strains of *P. aeruginosa* in the conditions tested was generally lower than the $K_d$ of the PCN-NHR-86 binding equilibrium. Previous studies have found that *P. aeruginosa* can produce greater quantities of PCN under other growth conditions[25]. Additionally, pathogen-mediated killing of *C. elegans* may occur too rapidly in the “fast kill” assay to resolve hypersusceptibility phenotypes. It is also possible that other signaling pathways in *C. elegans* can compensate for the loss of *nhr-86*.

# STAR Methods

## RESOURCE AVAILABILITY

**Lead Contact—**Further information requests for resources and reagents should be directed to and will be fulfilled by the lead contact, Read Pukkila-Worley (read.pukkila-worley@umassmed.edu).

**Material availability—**Strains and reagents generated in this study are available upon request.

### Data and code availability

- The mRNA-seq datasets have been deposited at NCBI Gene Expression Omnibus and are publicly available as of the date of publication. Accession numbers are listed in the key resources table. All other data are available in the manuscript and the accompanying Table S3, which contains all source data and statistical tests used.
- This paper does not report original code.
- Any additional information required to reanalyze the data reported in this paper is available from the lead contact upon request.

## EXPERIMENTAL MODEL AND SUBJECT DETAILS

***C. elegans* strains—**The previously published *C. elegans* strains used in this study were: N2 Bristol[77], AU307 *agIs44* [*irg-4*p::*gfp*::*unc-54*-3'UTR*; myo-2*p::*mCherry*][41], AY101 *acIs101* [p*DB09.1(irg-5*p::*gfp)*; pRF4(*rol-6(su1006)*)][81], VL491 *nhr-86(tm2590)*[50], VL648 *unc-119(ed3)* III; wwIs22[*nhr-86*p::*nhr-86*ORF::*gfp unc-119*(+)][50], RPW137 *nhr-86(ums12)*[39], RPW99 *nhr-86(tm2590)*; *agIs44*[39], RPW106 *nhr-86(tm2590)*; *acIs101*[39], RPW165 *nhr-86(ums12)*; *agIs44*[39], SJ4100 *zcIs13* [*hsp-6*::*gfp + lin-15(+)*][82], CA1200 *ieSi57* [*eft-3p*::*TIR1*::*mRuby*::*un54 3'UTR + Cbr-unc-119(+)*][51], OP318 *unc-119(ed3)*; *wgIs318*[*nhr-12*::*TY1*::*EGFP*::*3xFLAG(92C12)+unc-119(+)*][56], MGH167 *sid-1(qt9); aIxIs9* [*vha-6*p::*sid-1*::SL2::GFP][19]. The strains developed in this study were: RPW423 *umsEx88*[*cyp-35C1p*::*gfp*::*unc-54–3'UTR; myo-2p*::*mCherry*], RPW348 *nhr-86(ums64[NHR-86*::*AID])*; ieSi57, RPW424 *nhr-86(ums65[3xFLAG*::*NHR-86])*; ieSi57, RPW427 *nhr-86(ums66[3xFLAG*::*NHR-86*::*AID])*; ieSi57, RPW191 *nhr-86(ums14[3xFLAG*::*NHR-86])*, RPW401 *nhr-86(ums14[3xFLAG*::*NHR-86])*; *agIs44*, RPW430 *nhr-86(ums67[3xFLAG*::*NHR-86[F379H]])*;*agIs44*.

***C. elegans* growth conditions—***C. elegans* strains were maintained on standard nematode growth medium (NGM) plates [0.25% Bacto peptone, 0.3% sodium chloride, 1.7% agar (BD Bacto), 5 μg/mL cholesterol, 25 mM potassium phosphate pH 6.0, 1 mM magnesium sulfate, 1 mM calcium chloride] with *E. coli* OP50 as a food source, as described[77].

**Bacterial strains—**Bacteria used in this study were *Escherichia coli* (*E. coli*) OP50, *E. coli* DH5α, *E. coli* HT115(DE3), and *Pseudomonas aeruginosa* strains PA14[79], PAO1[73],

PAK[73], PA14 Δ*phzA1-G1* Δ*phzA2-G2* (Δ*phz*)[49], PA14 Δ*gacA*[7], and PA14 transposon mutants[80]. PA14 Δ*rhlR*, PA14 Δ*lasR* and PA14 Δ*pqsR* were obtained from Fred Ausubel.

**Bacterial growth conditions—***E. coli* OP50 were grown in LB broth supplemented with 0.175 mg/mL streptomycin at 37°C for 16–18 hrs at 250 rpm. *P. aeruginosa* strains were grown in LB broth at 37°C for 14 hrs at 250 rpm. LB was supplemented with gentamycin at a final concentration of 50 μg/mL where indicated.

## METHODS

**Feeding RNAi NHR screen—**Knockdown of target genes was performed by feeding *C. elegans E. coli* HT115 expressing dsRNA targeting the gene of interest, as previously described[78,93,94]. In brief, HT115 bacteria expressing dsRNA targeting genes of interest were grown in Lysogeny broth (LB) Lennox medium containing 50 μg/mL ampicillin overnight with shaking (250 rpm) at 37 °C. Overnight cultures were seeded onto NGM containing 5 mM isopropyl β-D-1-thiogalactopyranoside (IPTG) and 50 μg/mL carbenicillin and incubated at 37 °C for 16 hours, after which synchronized L1 animals were transferred to bacterial lawns and allowed to grow until the L4 stage.

We identified 274 nuclear hormone receptors that contained either an NHR zinc finger domain or an NHR ligand binding domain in the most recent release of the *C. elegans* genome (WS282) that were likely transcribed into protein. RNAi clones for 190 of these 274 genes were obtained from a previously-characterized library that was shared with us as a gift from Albertha J.M. Walhout[95]. 73 RNAi clones were obtained from either the Ahringer, Ahringer Supplemental, or Vidal RNAi libraries[96,97]. For 9 other RNAi clones, either the entire coding region of the gene or the largest exon for each gene was amplified by PCR using *C. elegans* coding DNA or genomic DNA as the template, respectively (See Table S4 for the primer list). PCR products were cloned into the RNAi expression vector L4440 using NEBuilder HiFi DNA Assembly (New England Biolabs #E2621), transformed into *E. coli* HT115, and selected on LB containing 5 μg/mL tetracycline and 50 μg/mL ampicillin, as previously described[42]. Transformants were then grown in LB containing 50 μg/mL ampicillin and frozen in a 96-well plate in 15% glycerol. Immediately prior to performing the screen, RNAi clones were stamped from frozen 96-well plates onto LB agar plates containing 50 μg/mL ampicillin and 5 μg/mL tetracycline. The source of the RNAi clones is summarized in Table S5. All clones were confirmed by Sanger sequencing.

For the RNAi screen, *C. elegans irg-4*p::*gfp* transcriptional reporter strains were grown from the L1 to L4 stage on HT115 *E. coli* expressing dsRNA targeting 271 of 274 *C. elegans* NHR genes in the genome. In brief, each well in a 24-well plate containing RNAi agar medium was seeded with 50 μL 5X concentrated overnight culture in M9 buffer of each RNAi clone. Seeded RNAi plates were then incubated overnight at 37 °C. Approximately 50 L1 synchronized *C. elegans irg-4*p::*gfp* transcriptional reporter animals were then dropped onto each bacterial clone and grown until the L4 stage. Animals were then transferred by washing with M9 to 24-well plates containing 25 μg/mL (112 μM) PCN and seeded with 50 μL *E. coli* OP50 for 20 hours. GFP induction was assessed by two independent observers.

RNAi clones corresponding to two *nhr* genes (*nhr-86* and *nhr-12*) abrogated the induction of *irg-4*p::*gfp* by PCN and displayed no defects in growth or development. Three RNAi clones were identified that suppressed *irg-4*p::*gfp* induction by PCN and had negative pleotropic effects on worm growth and development, and, for this reason, were not chosen for further study. A subsequent qRT-PCR analysis revealed that *irg-4* induction by PCN was not affected in the *nhr-12(tm1038)* mutant, indicating that *nhr-12* was a false positive hit in this screen (Fig. S2Q). PCN-mediated induction of *C. elegans irg-4*p::*gfp* was abrogated in *nhr-86(tm2590)* and *nhr-86(ums12)* mutants (Fig. 2C) and degradation of NHR-86 protein abrogated the induction of *irg-4* by PCN in a qRT-PCR experiment (Fig. 2D). Therefore, *nhr-86* was selected for further study. NHR-12, the closest related paralog to NHR-86, was used as a negative control in the CETSA experiment (Fig. 3F and 3G).

### *C. elegans* and *P. aeruginosa* strain construction

**Strain construction by CRISPR/Cas genome editing.:** All CRISPR genome editing was performed as previously described[98,99]. CRISPR-Cas9 editing with ssODN homolog directed repair was used to tag *nhr-86* with an auxin-inducible degron tag in animals carrying the *ieSi57* transgene, which expresses TIR1 protein in all somatic cells. Animals containing the NHR-86$^{F379H}$ mutation were generated in *nhr-86(ums14[3xFLAG::NHR-86]);agIs44* animals using CRISPR-Cas12 directed editing with ssODN homolog directed repair. All CRISPR reagents were purchased from Integrated DNA Technologies. Target guide sequences were selected using the CHOPCHOP web tool[100]. Single-stranded oligodeoxynucleotide (ssODN) repair templates contained indicated edits, deletions or insertions with 35 bp flanking homology arms. Cas9- and Cas12a-crRNA guide and ssODN sequences are listed in Table S4. The F1 progeny were screened for Rol phenotypes 3 to 4 days after injection and then for indicated edits using PCR and Sanger sequencing. Primer sequences used for genotyping are listed in Table S4.

**Construction of cyp-35C1p::gfp transgenic reporter animals.:** Animals carrying the *umsEx88* transgene were constructed as previously described[41]. Briefly, the region 1000 bp upstream of the *cyp-35C1* 5'UTR was PCR amplified, digested with HindIII and XbaI, and ligated into the *gfp* containing vector pPD95.75. Young adult N2 animals were microinjected with 25 ng/μL *umsEx88* construct along with 5 ng/μL *myo-2*p::*mCherry* co-injection marker. Primer sequences are listed in Table S4.

**Construction of P. aeruginosa pqsE overexpression strain.:** *P. aeruginosa pqsE* was amplified by PCR from *P. aeruginosa* PA14 DNA and cloned into the broad host range vector pHERD30T using NEBuilder HiFi DNA Assembly (New England Biolabs). Recombinant plasmids were propagated in *E. coli* DH5α cells and maintained with 50 μg/mL gentamycin selection. *P. aeruginosa* strains were transformed with *pqsE* constructs by electroporation and selected on LB agar containing 50 μg/mL gentamycin, as previously described[101]. Primer sequences are listed in Table S4.

**Studies with *C. elegans* GFP-based transcriptional reporters—**Immune and detoxification transcriptional reporter assays were performed as previously described[8,39]. We previously observed that induction of GFP in the transcriptional reporter *irg-4*p::*gfp* was

more robust when the nematode strains were grown on NGM media without supplemented cholesterol[8]. Thus, for the studies that utilized *C. elegans irg-4*p::*gfp* animals, NGM was prepared without cholesterol supplementation, and 0.1% ethanol was added to maintain an equivalent ethanol concentration. Single colonies of *P. aeruginosa* strains PA14, PA14 *Δphz*, PA14 transposon mutants, and *pqsE* overexpression strains were grown in 3 mL of LB (for PA14 and PA14 *Δphz*) or LB containing 50 μg/mL gentamicin (for PA14 transposon mutants and *pqsE* overexpression strains) at 37 °C for 14 hours at 250 rpm. 10 μL of culture was then seeded onto "slow-kill" agar (0.35% Bacto-peptone, 0.3% sodium chloride, 1.7% agar, 5 μg/mL cholesterol, 25 mM potassium phosphate, 1 mM magnesium sulfate, 1 mM calcium chloride), allowed to dry, and incubated at 37 °C for 24 hours followed by 25 °C for 24 hours. *E. coli* OP50 was the uninfected control. Phenazines were added to cooled media at the following final concentrations in 1% DMSO, unless otherwise noted: PCA (112 μM, 25 μg/mL), PCN (112 μM, 25 μg/mL), PYO (119 μM, 25 μg/mL), 1-HP (25 μM, 5 μg/mL). Of note, 1-HP was lethal to *C. elegans* when supplemented at a similar concentration as the other phenazines. Thus, we performed 1-HP supplementation with the highest concentration that did not affect animal survival in our assay. *P. aeruginosa Δphz* or *E. coli* OP50 were directly seeded onto phenazine-supplemented plates and dried. For *P. aeruginosa Δphz*, lawns were grown at 37 °C for 24 hours, followed by 25 °C for 24 hours. Around 50–100 *C. elegans* transcriptional reporter animals at the L4 stage were transferred to each bacterial lawn, prepared as described above. Images were taken 20 to 24 hours post-exposure, as described below.

**Microscopy and image analysis—**Nematodes were mounted onto 2% agarose pads, paralyzed with 50 mM tetramisole (Sigma) and imaged using a Zeiss AXIO Imager Z2 microscope with a Zeiss Axiocam 506 mono camera and Zen 2.3 (Zeiss) software. GFP fluorescence in the *irg-4*p::*gfp* transcriptional reporters after infection with *P. aeruginosa* mutants was quantified using the Lionheart FX Automatic Microscope (BioTek Instruments) under a 4X objective. After infection for 24 hours, ~50 animals were washed three times in M9 buffer containing 0.01% Triton X-100 and transferred to black-sided clear bottom 96-well plates containing 200 μL of 50 mM tetramisole. Animals were allowed to settle for 5 minutes. Individual animals were identified in each well, and mean GFP fluorescence intensity was quantified per animal using the Gen5 software (BioTek Instruments).

**Gene expression analyses and bioinformatics—**RNA-sequencing and data analysis were performed as previously described[8]. Briefly, synchronized N2 L1 stage *C. elegans* were grown to the L4 stage on NGM plates seeded with *E. coli* OP50 and transferred by washing with M9 to *P. aeruginosa, P. aeruginosa* Δ*phz*, or *E. coli* OP50 for 4 hours. For the NHR-86 RNA-seq experiment, synchronized L1 stage N2 wild-type animals were grown to L4 on either HT115 L4440 Control RNAi bacteria or HT115 *nhr-86(RNAi)* bacteria. L4 stage animals were then transferred to *E. coli* OP50-seeded agar plates containing solvent control (0.5% DMSO) or 25 μg/mL PCN for 4 hours. For both RNA-seq experiments, animals were harvested by washing with M9, RNA was isolated using TriReagent (Sigma-Aldrich), column purified (Qiagen), and analyzed by 100 bp paired-end mRNA-sequencing using the BGISEQ-500 platform (BGIAmericasCorp) with >20 million reads per sample. The quality of raw sequencing data was evaluated by FastQC (version 0.11.5), and clean

reads were aligned to the *C. elegans* reference genome (WBcel235) and quantified using Kallisto (version 0.45.0)[87]. Differentially expressed genes were identified using Sleuth (version 0.30.0)[88]. Pearson correlation statistical analysis was performed using Prism 9.0. Heatmaps of differentially expressed genes were generated using pheatmap (version 1.0.12). Gene set enrichment analysis of RNA-seq was performed using WormCat[90] for annotation of *C. elegans* gene categories and GSEA (version 4.2.3)[89] for assessing mitochondrial transcriptional signature in the RNA-seq experiment with PCN.

Gene set enrichment analysis of RNA-seq was performed using GSEA (version 4.2.3)[89] with a custom gene set database of *C. elegans* genes induced during infection with pathogen (*S. aureus*[102], *E. faecalis*, *E. carotovora*, *P. luminescens*, *S. marcescens*[103], and *S. flexneri*[104].

For the qRT-PCR studies, RNA was reverse transcribed to cDNA using the iScript cDNA Synthesis Kit (Bio-Rad) and analyzed using a CFX384 machine (Bio-Rad) using previously published primers[7,39,42]. All values were normalized against the geometric mean of control genes *snb-1* and *act-3*. Relative expression was calculated using the Pfaffl method[105].

**Chromatin Immunoprecipitation qPCR—**ChIP-qPCR was performed as previously described[39,106] with modification. Briefly, 80,000–100,000 synchronized L1 N2 or VL648 NHR-86::GFP[50] were grown to the L4 stage on NGM plates seeded with 20x E. coli OP50. Animals were transferred by washing with M9 to either solvent control (1% DMSO) or PCN (100 μg/mL) plates seeded with *E. coli* OP50 for 4 hours at 25 °C. Animals were harvested in M9, washed in M9 three times to remove bacteria, washed with PBS once, frozen as small droplets in liquid nitrogen, and placed at −80 °C until processing. Animals were mechanically disrupted by grinding frozen droplets to a fine powder in a mortar and pestle that was pre-chilled in liquid nitrogen. The powder was suspended and crosslinked in 1% formaldehyde (Thermo Fisher Scientific, #28908) (20,000 animals/mL) for 10 minutes at room temperature and quenched with 125 mM glycine. Samples were washed with PBS, resuspended in ChIP lysis buffer (50 mM Hepes–KOH pH 7.5, 300 mM NaCl, 1 mM EDTA, 1% (v/v) Triton X-100, 0.1% (w/v) sodium deoxycholate, 0.5% (v/v) N-Lauroylsarcosine, and 1x HALT protease inhibitor), and chromatin sheared using a Bioruptor UCD-200 for 15 cycles (30 s on, 30 s off) to obtain 500–1000 bp DNA fragments. 50 μL of input sample was removed from sheared lysates. Sheared lysates (2 mg) were immunoprecipitated with 5 μg/mL anti-GFP antibody (Thermo Fisher Scientific, #11814460001) bound to protein G Dynabeads (Invitrogen, #10004D) at 4 °C overnight. Immune complex bound beads were washed with ChIP lysis buffer twice, ChIP lysis buffer containing 800 mM NaCl once, ChIP wash buffer (10 mM Tris-HCl pH 8.0, 250 mM LiCl, 0.5 % NP-40, 0.5 % sodium deoxycholate, 1 mM EDTA) twice, and TE containing salt (10 mM Tris-HCl pH 8.0, 1 mM EDTA, 50 mM NaCl) once. Chromatin was eluted off the beads with ChIP elution buffer (50 mM Tris–HCl pH 8.0, 1 mM EDTA, 1% SDS), and crosslinks were reversed by incubating samples at 65 °C overnight. DNA was treated with 10 μL RNase A (100 mg/mL) (Qiagen, #191010) for 2 hours at 37 °C, 10 μL Proteinase K (20 mg/mL) (New England BioLabs) for 1 hour at 55 °C, and extracted with phenol:chloroform:isoamyl alcohol, ethanol precipitated, and resuspended in elution buffer (EB) (Qiagen). qPCR was performed on input and immunoprecipitated samples using primers designed upstream of the

transcription start site and at an intergenic region. All data are presented as percent of input DNA. Primer sequences used for qPCR are listed in Table S4.

**Immunoblot analyses—**Protein lysates for cellular thermal shift (CETSA) experiments were prepared as described below. For all other immunoblots, protein lysates were prepared using a Teflon Dounce homogenizer from 2,000 *C. elegans* grown to the L4 larval stage on NGM plates seeded with *E. coli* OP50, as previously described[8]. LDS Sample Buffer (Thermo Fisher Scientific) was added to a concentration of 1X with 1% β-mercaptoethanol. All samples were incubated at 70 °C for 10 minutes. Total protein from each sample was resolved on NuPage Bis-Tris 4–12% gels (Life Technologies), transferred to 0.2 μM nitrocellulose membranes (Bio-Rad), and blocked with 5% milk in 1x TBS + 0.2% Tween-20 for one hour. Blots were then probed with a 1:1000 dilution of mouse monoclonal anti-FLAG M2 (Sigma, #F1804), mouse monoclonal anti-alpha-Tubulin (Sigma, #T5168), or rabbit monoclonal anti-Actin (Abcam, #ab179467) overnight at 4 °C. Anti-mouse IgG-HRP (Abcam, #ab6789) or anti-rabbit IgG-HRP (Cell Signaling Technology, #7074) secondary antibodies were used at a dilution of 1:10,000 to detect the primary antibodies. Blots were then developed with the addition of SuperSignal™ West Pico PLUS Chemiluminescent Substrate (Thermo Fisher Scientific) and visualized using a ChemiDoc MP Imaging System (Bio-Rad). Band intensities were quantified using ImageJ (Fiji).

**NHR-86 Ligand-binding domain expression and purification—**The NHR-86 ligand-binding domain (NHR-86, isoform a, amino acid residues 130–405), codon optimized for *E. coli*, was synthesized by GenScript, amplified by PCR, digested with *Bam*HI and *Xho*I, and ligated into the vector pSMT3 containing a cleavable N-terminus His6x-SUMO tag[84]. The NHR-86 ligand binding domain mutant containing the F379H mutation was introduced by PCR amplification using primers (Table S4) containing the F379H mutation and the pSMT3::NHR-86(LBD) construct as the template (0.5 ng/μL). Template DNA was digested and PCR ligated using the Q5 Site-Directed Mutagenesis Kit (New England BioLabs) with room temperature incubation for 10 minutes. 1 μL of ligations were transformed into chemically competent *E. coli* BL21(DE3) cells and maintained with 50 μg/mL kanamycin selection. For protein expression, a single colony was inoculated into 25 mL LB containing 50 μg/mL kanamycin and grown overnight. Overnight cultures were subcultured to an $OD_{600}$ of 0.05 in Terrific Broth (2.4% yeast extract, 2% bacto tryptone, 0.4% glycerol, 17 mM $KH_2PO_4$, 72 mM $K_2HPO_4$) containing kanamycin and grown at 37 °C with 180 rpm shaking until an $OD_{600}$ of 0.6–0.8. Cells were then placed on ice for 15 minutes. After cooling, isopropyl β-D-1-thiogalactopyranoside (IPTG) was added to a final concentration of 0.5 mM and cultures were incubated for 18 hours at 16 °C with shaking at 180 rpm. Cultures were harvested by centrifugation at 4,000 rpm for 20 minutes at 4 °C, resuspended in binding buffer [50 mM $NaH_2PO_4$ pH 8.0, 500 mM NaCl, 0.001% Tween20, 5 mM β-mercaptoethanol, 10% glycerol (w/v), 5 mM imidazole], flash-frozen in liquid $N_2$, and placed at −80 °C until purification.

To purify the NHR-86(LBD) and NHR-86(LBD)$^{F379H}$, samples were thawed and sonicated on ice with a Qsonica Q700 microtip sonicator at an amplitude of 30 for 20 seconds (1 sec on, 1 sec off) followed by 20 seconds off for 12 cycles total. Crude lysate was centrifuged

at 10,000 rpm for 30 minutes at 4°C. The soluble fraction was filtered through a 0.45-μM filter and bound to a pre-equilibrated Ni-NTA resin (Qiagen, #30210) by incubating at 4 °C for 1 hour. Bound resin was placed in a column and allowed to flow by gravity. The column was washed with 20 column volumes of wash buffer [50 mM $NaH_2PO_4$ pH 8.0, 500 mM NaCl, 0.001% Tween20, 5 mM β-mercaptoethanol, 10% glycerol (w/v), 20 mM imidazole], and protein was eluted with 5 column volumes of elution buffer [50 mM $NaH_2PO_4$ pH 8.0, 500 mM NaCl, 0.001% Tween20, 5 mM β-mercaptoethanol, 10% glycerol (w/v), 250 mM imidazole]. Protein was dialyzed overnight with 50 mM $NaH_2PO_4$ pH 8.0, 300 mM NaCl, 10% glycerol (w/v). His6-SUMO tag was removed by incubating 7 units of Ulp1 protease (Sigma, #SAE0067) per mg protein with 0.5-mM DTT overnight at 4 °C. Ulp1 protease and His6-SUMO tag were removed by applying protein digestion to a pre-equilibrated Ni-NTA (Qiagen, #30210) column and collecting the flow-through, which was concentrated, dialyzed overnight, flash-frozen in liquid $N_2$, and stored at −80 °C.

## Protein biophysical assays

**Cellular Thermal Shift Assay (CETSA).:** For each assay, approximately 100,000–200,000 L4 3xFLAG::NHR-86 or 3xFLAG::NHR-86$^{F379H}$ animals were resuspended in 1–2 mL of PBS supplemented with HALT protease inhibitor cocktail and lysed using a Teflon Dounce homogenizer on a rotor until all animals were visibly lysed. Cellular debris was removed by centrifugation at 16,000 rpm for 20 minutes at 4°C. Protein in the clarified whole-cell lysate was quantified using the *DC* Protein Assay (Bio-Rad) and adjusted to 10 mg/mL. The whole-cell lysate was then divided into 1.5 mL microcentrifuge tubes and treated with either 1–2% DMSO, 400–500 μM PCA, 400–500 μM PCN, or 70 μM R24 for 15–60 minutes at room temperature. While incubating, 50 μL of lysate from each condition was distributed into PCR tube strips and exposed to increasing temperatures (25–65°C) for 3 minutes on a Bio-Rad C1000 Touch Thermal Cycler, cooled to room temperature for 3 minutes, and immediately placed on ice. Samples were transferred to 1.5-mL microcentrifuge tubes and spun at 20,000 *g* for 20 minutes at 4 °C to remove precipitated proteins. The supernatants for each temperature and condition were carefully transferred to new tubes – without disturbing the pellet or touching the sides of the tubes – containing LDS Sample Buffer (Thermo Fisher) and 1% β-mercaptoethanol. Samples were then assessed for the presence of 3xFLAG::NHR-86 or 3xFLAG::NHR-86$^{F379H}$ using immunoblot analysis, as described above.

**Intrinsic tryptophan assays.:** Measurement of NHR-86(LBD) and NHR-86(LBD)$^{F379H}$ tryptophan fluorescence was performed as previously described with modification[54,107]. Briefly, 2 μM NHR-86(LBD) or NHR-86(LBD)$^{F379H}$ protein was incubated with either DMSO (1% final) or increasing concentrations of R24, PCN, or PCA in a 20 μL final volume. Samples were incubated at room temperature for 1 hour in 384 black-walled, round-bottom plates (Corning, #3676). Tryptophan fluorescence was measured using a Molecular Devices SpectraMax iD5 instrument with the following settings: excitation at 295 nm, emission at 340 nm, PMT low, integration 100 ms.

To correct for non-specific tryptophan quenching, each compound was simultaneously incubated with 10 μM N-acetyl-L-trytophanamide (NATA) (Sigma, #A6501), a tryptophan

analog. The fraction of fluorescence decrease at each compound concentration in NATA was multiplied by the protein solvent control condition, and the measured protein fluorescence at each corresponding compound concentration was then corrected by this factor. Data points for each compound were fit using the following non-linear curve fitting equation:

$$Y = Yo * \left(1 - \left(\frac{(Pt + X + Kd) - \left(\left((Pt + X + Kd)^2\right) - 4 * Pt * X\right)^{0.5}}{2 * Pt}\right)\right) + Yf\left(\frac{(Pt + X + Kd) - \left(\left((Pt + X + Kd)^2\right) - 4 * Pt * X\right)^{0.5}}{2 * Pt}\right)$$

Yo = protein fluorescence intensity with solvent control

Pt = protein concentration

X = concentration of ligand

$K_d$ = equilibrium dissociation constant

**NHR-86 depletion by auxin-inducible degron—**For NHR-86 depletion using the auxin-inducible degron, wild-type and NHR-86::AID animals were treated with 50 μM auxin naphthaleneacetic acid (NAA) (PhytoTech Labs) from the L1 to the L4 larval stage and during all experimental conditions. For these studies, a transgenic *C. elegans* strain was used that expresses TIR1 in all tissues under the *eft-3* promoter[51]. To avoid NAA impacts on bacterial growth and metabolism, NAA was added on top of bacterial lawns and allowed to diffuse into plates for 2 hours prior to use. We confirmed that NHR-86::AID was degraded during auxin treatment by using CRISPR genome editing to introduce a 3X FLAG tag into the NHR-86::AID strain and immunoblotted for 3xFLAG::NHR-86::AID with an anti-FLAG antibody as described below (Fig. S2C).

***C. elegans* pathogenesis and development assays—**"Fast-killing" *P. aeruginosa* infection experiments were performed as previously described[58,59]. In brief, a single colony of *P. aeruginosa* was inoculated into 3 mL of LB Lennox medium and allowed to incubate at 37 °C for 14 hours at 250 rpm. 5 μL of this culture was spread in the center of 35-mm tissue culture plates containing 4 mL of fast-kill agar (*i.e.*, PSG agar) (1% Bacto-peptone, 1% glucose, 1% sodium chloride, 150 mM sorbitol, 1.7% Bacto-agar). Plates were incubated for 24 hours at 37 °C followed by 24 hours at 25 °C. Approximately 40 L4 larval stage nematodes were transferred to the pseudomonal lawns on fast-kill plates. Dead nematodes were scored at 2, 4, 8 or 24 hours by assessing movement after tapping on the heads with a platinum wire. For the "fast kill" assays with PCN supplementation, agar plates were prepared as above. Following a previously described protocol[58], the bacterial lawn was scraped from the plates after 48 hours of *P. aeruginosa* growth, the agar was melted, and 100 μg/mL PCN or DMSO (1% final) was added to the liquid media. The plates were then re-poured. 20 μL of 20x *E. coli* OP50 was added to plates and allowed to dry. L4 *C. elegans* were then washed with M9 to NGM plates containing 100 μg/mL PCN or DMSO (1% final), prepared as described for studies with transcriptional reporters, for 2 hours before being picked to supplemented fast-kill plates. Three trials of each pathogenesis assay were

performed. Sample sizes, four-hour survival, and p-values for all trials are shown in Table S2.

"Slow-killing" *P. aeruginosa* infection experiments (Fig. S5B) were performed as previously described[61,108]. In brief, *P. aeruginosa* was grown as described above and 10 μL overnight culture was spread onto the center of 35-mm tissue culture plates containing 4 mL slow-kill agar (0.35% Bacto-peptone, 0.3% sodium chloride, 1.7% agar, 5 μg/mL cholesterol, 25 mM potassium phosphate, 1 mM magnesium sulfate, 1 mM calcium chloride). Plates were then incubated for 24 hours at 37°C followed by 24 hours at 25°C. Wild-type and *nhr-86(RNAi) C. elegans* pre-treated with 1% DMSO or 100 μg/mL PCN for 2 hours at the L4 stage were then transferred to *P. aeruginosa* slow-kill plates. Dead animals were scored twice daily until completion. Three trials of the assay were performed. Sample sizes, mean survival and p-values for all trials are shown in Table S2.

Assays assessing the growth of *C. elegans* were performed as described with some modifications[42,108]. Briefly, CA1200 and NHR-86::AID animals were grown in the presence of 50 μM auxin until the L4 (Fig. 5C) or gravid (Fig. 5D) stage. Animals were then transferred onto NGM plates with 50 μM auxin and without exogenous cholesterol. Animals were photographed after 96 hours (Fig. 5C) or scored for the percent of live animals after 72 hours (Fig. 5D). Lawn occupancy assays were performed as previously described[108].

## Quantification of phenazines

**High-Performance Liquid Chromatography-Ultraviolet spectroscopy (HPLC-UV) and Liquid Chromatography/Mass-Spectrometry (LC-MS).:** Quantification of phenazines was performed as previously described[109]. In brief, agar plates grown with each pseudomonal strain were diced into 5–10 mm cubes and transferred to 50 mL polypropylene tubes containing 5 mL HPLC-grade methanol. Samples were nutated overnight to extract phenazines from both the agar and bacterial biofilms.

Supernatants from methanol-extracted samples were filtered through 0.22 μm cellulose Spin-X columns (Thermo Fisher Scientific 07–200-386), and the filtrates were stored at −80 °C until HPLC-UV analysis. On the day of HPLC-UV analysis, 100 μL of supernatant were transferred to HPLC screw-top vials with fixed inserts (Agilent Technologies 5188–6592). Phenazines were quantified using the Agilent 1260 Infinity HPLC with a biphenyl column (Kinetex 00F-4622-E0, 4.6 × 150 mm, 2.6 μm) and a 20 μL injection volume. A gradient method was used, as described previously[109]. Phenazines were quantified by integrating the peaks observed at an absorbance of 366 nm, and phenazines were identified by comparing the retention times to the phenazine standards. All retention times and phenazine quantifications can be found in Table S3.

For Figure S1M, *P. aeruginosa* PA14 wild-type and *phzH*::Tn mutants were grown as described above. Bacteria were scraped off the surface of the agar and $OD_{600}$ values were quantified. The agar for each strain was cut up into small pieces and flash-frozen directly in liquid nitrogen. Samples were then pulverized on a Mixer Mill MM 400 (Retsch) under cryogenic conditions at 30 Hz for 90 seconds. Pulverized agar samples were stored at −80 °C until LC-MS/MS analysis.

Phenazines were extracted using methanol and chloroform. The organic phase was dried under nitrogen gas and resuspended in methanol. Samples were filtered through a 0.2 μm PVDF filter and assessed on a Thermo Scientific Ultimate 3000 HPLC system coupled with a Thermo Scientific TSQ Quantiva triple quadrupole mass spectrometer with a Waters Acquity BEH C18 Column and Waters Acquity BEH C18 VanGuard pre-column. The sample injection volume was 2 μL. Mobile phase A consisted of 0.1% formic acid in water, and mobile phase B consisted of 0.1% formic acid in acetonitrile. The gradient started at 35% B for 1.5 min and increased to 99% B over the course of 7 min at a flow rate of 0.25 mL/minute. MS analysis was performed with an electrospray ionization source with a capillary voltage of +3.7 kV. The following was used for the sheath gas: 40 Arb; Aux gas: 10 Arb, vaporizer temperature: 250 °C, ion transfer tube temperature: 325 °C. The multiple reaction monitoring (MRM) parameters were the following: duty cycle time 0.3s, CID gas pressure 1.5 mTorr, Q1 resolution (full width at half maximum, FWHM) 0.7, Q3 resolution (FWHM) 0.7. Quantification of phenazines can be found in Table S3.

**Molecular modelling and molecular dynamics simulations—**AlphaFold-Multimer[92] was used to predict the homodimeric structure of full length NHR-86. The model was optimized using Protein Preparation Wizard (Schrödinger v.19–4) to determine protonation states at pH 6.0 and optimize the hydrogen bonding network. A restrained minimization was performed using the OPLS2005 force field[110] within an RMSD of 0.3 Å. To determine an optimal binding pocket, SiteMap[111] (Schrödinger v.19–4) was used with default settings, and the final binding pocket was chosen based on the size, hydrophobicity, and hydrophilicity. Each ligand of interest was converted to an energy minimized 3D molecular structure using LigPrep (Schrödinger v.19–4), and docked within the binding pocket using Glide[112] (Schrödinger v.19–4). Energy minimization was conducted for ligand poses with highest docking scores. A multistage 100 ns molecular dynamics simulation with randomized starting velocities was performed for each ligand-protein complex using Desmond (Schrödinger v.19–4). Forcefield parameters were assigned using OPLS3[113]. Each complex was solvated in a cubic box with at least 15 Å between any solute atom and the periodic boundaries using the TIP3P water model. Charges were neutralized using sodium and chloride ions, and additional counterions were added up to a concentration of 0.15 M. MM/GBSA calculations were carried out using 100 frames of the simulation using a custom script. Structural figures and movies were generated using PyMOL (v. 2.3.4) and VMD (v. 1.9.4).

## QUANTIFICATION AND STATISTICAL ANALYSIS

Differences in the survival of *C. elegans* in the *P. aeruginosa* pathogenesis assays were determined with the log-rank test after survival curves were estimated for each group with the Kaplan-Meier method. OASIS 2 was used for these statistical analyses[86]. Statistical hypothesis testing was performed with Prism 9 (GraphPad Software) using methods indicated in the figure legends. Table S3 contains all source data and statistical analysis methods and results. Sample sizes, survival, and p-values for all trials are shown in Table S2.

## Supplementary Material

Refer to Web version on PubMed Central for supplementary material.

## Acknowledgements:

The authors acknowledge Brian Kelch, Ala Shaqra, and Joseph Magrino for reagents and helpful discussions regarding NHR-86 protein expression; Scott Shaffer, Janneke Icso, Shruti Choudhary and Paul Thompson for assistance with phenazine quantification; Albertha J.M. Walhout for the gift of RNAi bacteria clones; and Melanie Trombly and Merin MacDonald for critical reading of the manuscript. This research was supported by R01 AI130289 (to R.P.W.), R01 AI159159 (to R.P.W.), R21 AI163430 (to R.P.W.), an Innovator Award from the Kenneth Rainin Foundation (to R.P.W.), the Dan and Diane Riccio Fund for Neuroscience (to R.P.W.), F30 AI150127 (to N.D.P.), F30 DK127690 (to S.Y.T.), T32 AI132152 (to N.D.P.), T32 AI095213 (to S.Y.T.), T32 GM107000 (to N.D.P. and S.Y.T.), R01 AI150478 (to C.A.S.), R01 GM135919 (to C.A.S.), and R21 AI149716 (to C.A.S.). Some strains were provided by the *Caenorhabditis* Genetics Center, which is funded by the NIH Office of Research Infrastructure Programs (P40 OD010440).

## Inclusion and diversity

We support inclusive, diverse, and equitable conduct of research.

## References

1. Ausubel FM (2005). Are innate immune signaling pathways in plants and animals conserved? Nat Immunol 6, 973–979. 10.1038/ni1253. [PubMed: 16177805]
2. Brennan JJ, and Gilmore TD (2018). Evolutionary Origins of Toll-like Receptor Signaling. Mol Biol Evol 35, 1576–1587. 10.1093/molbev/msy050. [PubMed: 29590394]
3. Irazoqui JE, Urbach JM, and Ausubel FM (2010). Evolution of host innate defence: insights from *Caenorhabditis elegans* and primitive invertebrates. Nat Rev Immunol 10, 47–58. 10.1038/nri2689. [PubMed: 20029447]
4. Kim DH, and Ewbank JJ (2018). Signaling in the innate immune response. WormBook 2018, 1–35. 10.1895/wormbook.1.83.2.
5. Pukkila-Worley R, and Ausubel FM (2012). Immune defense mechanisms in the *Caenorhabditis elegans* intestinal epithelium. Curr Opin Immunol 24, 3–9. 10.1016/j.coi.2011.10.004. [PubMed: 22236697]
6. Fitzgerald KA, and Kagan JC (2020). Toll-like Receptors and the Control of Immunity. Cell 180, 1044–1066. 10.1016/j.cell.2020.02.041. [PubMed: 32164908]
7. Troemel ER, Chu SW, Reinke V, Lee SS, Ausubel FM, and Kim DH (2006). p38 MAPK regulates expression of immune response genes and contributes to longevity in *C. elegans*. PLoS Genet 2, e183. 10.1371/journal.pgen.0020183. [PubMed: 17096597]
8. Peterson ND, Icso JD, Salisbury JE, Rodriguez T, Thompson PR, and Pukkila-Worley R (2022). Pathogen infection and cholesterol deficiency activate the *C. elegans* p38 immune pathway through a TIR-1/SARM1 phase transition. Elife 11. 10.7554/eLife.74206.
9. Foster KJ, Cheesman HK, Liu P, Peterson ND, Anderson SM, and Pukkila-Worley R (2020). Innate Immunity in the *C. elegans* Intestine Is Programmed by a Neuronal Regulator of AWC Olfactory Neuron Development. Cell Rep 31, 107478. 10.1016/j.celrep.2020.03.042. [PubMed: 32268082]
10. Wu Z, Isik M, Moroz N, Steinbaugh MJ, Zhang P, and Blackwell TK (2019). Dietary Restriction Extends Lifespan through Metabolic Regulation of Innate Immunity. Cell Metab 29, 1192–1205 e1198. 10.1016/j.cmet.2019.02.013. [PubMed: 30905669]
11. Cao X, Kajino-Sakamoto R, Doss A, and Aballay A (2017). Distinct Roles of Sensory Neurons in Mediating Pathogen Avoidance and Neuropeptide-Dependent Immune Regulation. Cell Rep 21, 1442–1451. 10.1016/j.celrep.2017.10.050. [PubMed: 29117551]
12. Cao X, and Aballay A (2016). Neural Inhibition of Dopaminergic Signaling Enhances Immunity in a Cell-Non-autonomous Manner. Curr Biol 26, 2329–2334. 10.1016/j.cub.2016.06.036. [PubMed: 27524480]

13. Styer KL, Singh V, Macosko E, Steele SE, Bargmann CI, and Aballay A (2008). Innate immunity in *Caenorhabditis elegans* is regulated by neurons expressing NPR-1/GPCR. Science 322, 460–464. 10.1126/science.1163673. [PubMed: 18801967]
14. Anderson SM, and Pukkila-Worley R (2020). Immunometabolism in *Caenorhabditis elegans*. PLoS Pathog 16, e1008897. 10.1371/journal.ppat.1008897. [PubMed: 33031414]
15. Zugasti O, Bose N, Squiban B, Belougne J, Kurz CL, Schroeder FC, Pujol N, and Ewbank JJ (2014). Activation of a G protein-coupled receptor by its endogenous ligand triggers the innate immune response of *Caenorhabditis elegans*. Nat Immunol 15, 833–838. 10.1038/ni.2957. [PubMed: 25086774]
16. Pellegrino MW, Nargund AM, Kirienko NV, Gillis R, Fiorese CJ, and Haynes CM (2014). Mitochondrial UPR-regulated innate immunity provides resistance to pathogen infection. Nature 516, 414–417. 10.1038/nature13818. [PubMed: 25274306]
17. Dunbar TL, Yan Z, Balla KM, Smelkinson MG, and Troemel ER (2012). *C. elegans* detects pathogen-induced translational inhibition to activate immune signaling. Cell Host Microbe 11, 375–386. 10.1016/j.chom.2012.02.008. [PubMed: 22520465]
18. McEwan DL, Kirienko NV, and Ausubel FM (2012). Host translational inhibition by *Pseudomonas aeruginosa* Exotoxin A Triggers an immune response in *Caenorhabditis elegans*. Cell Host Microbe 11, 364–374. 10.1016/j.chom.2012.02.007. [PubMed: 22520464]
19. Melo JA, and Ruvkun G (2012). Inactivation of conserved *C. elegans* genes engages pathogen- and xenobiotic-associated defenses. Cell 149, 452–466. 10.1016/j.cell.2012.02.050. [PubMed: 22500807]
20. Pukkila-Worley R (2016). Surveillance Immunity: An Emerging Paradigm of Innate Defense Activation in *Caenorhabditis elegans*. PLoS Pathog 12, e1005795. 10.1371/journal.ppat.1005795. [PubMed: 27631629]
21. Singh J, and Aballay A (2019). Intestinal infection regulates behavior and learning via neuroendocrine signaling. Elife 8. 10.7554/eLife.50033.
22. Filipowicz A, Lalsiamthara J, and Aballay A (2021). TRPM channels mediate learned pathogen avoidance following intestinal distention. Elife 10. 10.7554/eLife.65935.
23. Singh J, and Aballay A (2019). Microbial Colonization Activates an Immune Fight-and- Flight Response via Neuroendocrine Signaling. Dev Cell 49, 89–99 e84. 10.1016/j.devcel.2019.02.001. [PubMed: 30827896]
24. Dorrestein PC, Mazmanian SK, and Knight R (2014). Finding the missing links among metabolites, microbes, and the host. Immunity 40, 824–832. 10.1016/j.immuni.2014.05.015. [PubMed: 24950202]
25. Saunders SH, Tse ECM, Yates MD, Otero FJ, Trammell SA, Stemp EDA, Barton JK, Tender LM, and Newman DK (2020). Extracellular DNA Promotes Efficient Extracellular Electron Transfer by Pyocyanin in *Pseudomonas aeruginosa* Biofilms. Cell 182, 919–932 e919. 10.1016/j.cell.2020.07.006. [PubMed: 32763156]
26. Meisel JD, Panda O, Mahanti P, Schroeder FC, and Kim DH (2014). Chemosensation of bacterial secondary metabolites modulates neuroendocrine signaling and behavior of *C. elegans*. Cell 159, 267–280. 10.1016/j.cell.2014.09.011. [PubMed: 25303524]
27. Sluder AE, and Maina CV (2001). Nuclear receptors in nematodes: themes and variations. Trends Genet 17, 206–213. [PubMed: 11275326]
28. Sluder AE, Mathews SW, Hough D, Yin VP, and Maina CV (1999). The nuclear receptor superfamily has undergone extensive proliferation and diversification in nematodes. Genome Res 9, 103–120. [PubMed: 10022975]
29. Taubert S, Ward JD, and Yamamoto KR (2011). Nuclear hormone receptors in nematodes: evolution and function. Mol Cell Endocrinol 334, 49–55. 10.1016/j.mce.2010.04.021. [PubMed: 20438802]
30. Sural S, and Hobert O (2021). Nematode nuclear receptors as integrators of sensory information. Curr Biol 31, 4361–4366 e4362. 10.1016/j.cub.2021.07.019. [PubMed: 34348120]
31. Magner DB, and Antebi A (2008). *Caenorhabditis elegans* nuclear receptors: insights into life traits. Trends Endocrinol Metab 19, 153–160. 10.1016/j.tem.2008.02.005. [PubMed: 18406164]

32. Watson E, and Walhout AJ (2014). *Caenorhabditis elegans* metabolic gene regulatory networks govern the cellular economy. Trends Endocrinol Metab 25, 502–508. 10.1016/j.tem.2014.03.004. [PubMed: 24731597]
33. Motola DL, Cummins CL, Rottiers V, Sharma KK, Li T, Li Y, Suino-Powell K, Xu HE, Auchus RJ, Antebi A, and Mangelsdorf DJ (2006). Identification of ligands for DAF-12 that govern dauer formation and reproduction in *C. elegans*. Cell 124, 1209–1223. 10.1016/j.cell.2006.01.037. [PubMed: 16529801]
34. Lin CJ, and Wang MC (2017). Microbial metabolites regulate host lipid metabolism through NR5A-Hedgehog signalling. Nat Cell Biol 19, 550–557. 10.1038/ncb3515. [PubMed: 28436966]
35. Folick A, Oakley HD, Yu Y, Armstrong EH, Kumari M, Sanor L, Moore DD, Ortlund EA, Zechner R, and Wang MC (2015). Aging. Lysosomal signaling molecules regulate longevity in *Caenorhabditis elegans*. Science 347, 83–86. 10.1126/science.1258857. [PubMed: 25554789]
36. Warnhoff K, Roh HC, Kocsisova Z, Tan CH, Morrison A, Croswell D, Schneider DL, and Kornfeld K (2017). The Nuclear Receptor HIZR-1 Uses Zinc as a Ligand to Mediate Homeostasis in Response to High Zinc. PLoS Biol 15, e2000094. 10.1371/journal.pbio.2000094. [PubMed: 28095401]
37. Vance RE, Isberg RR, and Portnoy DA (2009). Patterns of pathogenesis: discrimination of pathogenic and nonpathogenic microbes by the innate immune system. Cell Host Microbe 6, 10–21. 10.1016/j.chom.2009.06.007. [PubMed: 19616762]
38. Huang H, Shao X, Xie Y, Wang T, Zhang Y, Wang X, and Deng X (2019). An integrated genomic regulatory network of virulence-related transcriptional factors in *Pseudomonas aeruginosa*. Nat Commun 10, 2931. 10.1038/s41467-019-10778-w. [PubMed: 31270321]
39. Peterson ND, Cheesman HK, Liu P, Anderson SM, Foster KJ, Chhaya R, Perrat P, Thekkiniath J, Yang Q, Haynes CM, and Pukkila-Worley R (2019). The nuclear hormone receptor NHR-86 controls anti-pathogen responses in *C. elegans*. PLoS Genet 15, e1007935. 10.1371/journal.pgen.1007935. [PubMed: 30668573]
40. Pukkila-Worley R, Feinbaum R, Kirienko NV, Larkins-Ford J, Conery AL, and Ausubel FM (2012). Stimulation of host immune defenses by a small molecule protects *C. elegans* from bacterial infection. PLoS Genet 8, e1002733. 10.1371/journal.pgen.1002733. [PubMed: 22719261]
41. Pukkila-Worley R, Feinbaum RL, McEwan DL, Conery AL, and Ausubel FM (2014). The evolutionarily conserved mediator subunit MDT-15/MED15 links protective innate immune responses and xenobiotic detoxification. PLoS Pathog 10, e1004143. 10.1371/journal.ppat.1004143. [PubMed: 24875643]
42. Cheesman HK, Feinbaum RL, Thekkiniath J, Dowen RH, Conery AL, and Pukkila-Worley R (2016). Aberrant Activation of p38 MAP Kinase-Dependent Innate Immune Responses Is Toxic to *Caenorhabditis elegans*. G3 (Bethesda) 6, 541–549. 10.1534/g3.115.025650. [PubMed: 26818074]
43. Shapira M, Hamlin BJ, Rong J, Chen K, Ronen M, and Tan MW (2006). A conserved role for a GATA transcription factor in regulating epithelial innate immune responses. Proc Natl Acad Sci USA 103, 14086–14091. 10.1073/pnas.0603424103. [PubMed: 16968778]
44. Anderson SM, Cheesman HK, Peterson ND, Salisbury JE, Soukas AA, and Pukkila-Worley R (2019). The fatty acid oleate is required for innate immune activation and pathogen defense in *Caenorhabditis elegans*. PLoS Pathog 15, e1007893. 10.1371/journal.ppat.1007893. [PubMed: 31206555]
45. Williams P, and Camara M (2009). Quorum sensing and environmental adaptation in *Pseudomonas aeruginosa*: a tale of regulatory networks and multifunctional signal molecules. Curr Opin Microbiol 12, 182–191. 10.1016/j.mib.2009.01.005. [PubMed: 19249239]
46. Papenfort K, and Bassler BL (2016). Quorum sensing signal-response systems in Gram-negative bacteria. Nat Rev Microbiol 14, 576–588. 10.1038/nrmicro.2016.89. [PubMed: 27510864]
47. Mukherjee S, Moustafa D, Smith CD, Goldberg JB, and Bassler BL (2017). The RhlR quorum-sensing receptor controls *Pseudomonas aeruginosa* pathogenesis and biofilm development independently of its canonical homoserine lactone autoinducer. PLoS Pathog 13, e1006504. 10.1371/journal.ppat.1006504. [PubMed: 28715477]

48. Mavrodi DV, Bonsall RF, Delaney SM, Soule MJ, Phillips G, and Thomashow LS (2001). Functional analysis of genes for biosynthesis of pyocyanin and phenazine-1-carboxamide from *Pseudomonas aeruginosa* PAO1. J Bacteriol 183, 6454–6465. 10.1128/JB.183.21.6454-6465.2001. [PubMed: 11591691]
49. Dietrich LE, Price-Whelan A, Petersen A, Whiteley M, and Newman DK (2006). The phenazine pyocyanin is a terminal signalling factor in the quorum sensing network of *Pseudomonas aeruginosa*. Mol Microbiol 61, 1308–1321. 10.1111/j.1365-2958.2006.05306.x. [PubMed: 16879411]
50. Arda HE, Taubert S, MacNeil LT, Conine CC, Tsuda B, Van Gilst M, Sequerra R, Doucette-Stamm L, Yamamoto KR, and Walhout AJ (2010). Functional modularity of nuclear hormone receptors in a *Caenorhabditis elegans* metabolic gene regulatory network. Mol Syst Biol 6, 367. 10.1038/msb.2010.23. [PubMed: 20461074]
51. Zhang L, Ward JD, Cheng Z, and Dernburg AF (2015). The auxin-inducible degradation (AID) system enables versatile conditional protein depletion in *C. elegans*. Development 142, 4374–4384. 10.1242/dev.129635. [PubMed: 26552885]
52. Haynes CM, Yang Y, Blais SP, Neubert TA, and Ron D (2010). The matrix peptide exporter HAF-1 signals a mitochondrial UPR by activating the transcription factor ZC376.7 in *C. elegans*. Mol Cell 37, 529–540. 10.1016/j.molcel.2010.01.015. [PubMed: 20188671]
53. Deng P, Uma Naresh N, Du Y, Lamech LT, Yu J, Zhu LJ, Pukkila-Worley R, and Haynes CM (2019). Mitochondrial UPR repression during *Pseudomonas aeruginosa* infection requires the bZIP protein ZIP-3. Proc Natl Acad Sci U S A 116, 6146–6151. 10.1073/pnas.1817259116. [PubMed: 30850535]
54. Yammine A, Gao J, and Kwan AH (2019). Tryptophan Fluorescence Quenching Assays for Measuring Protein-ligand Binding Affinities: Principles and a Practical Guide. Bio Protoc 9, e3253. 10.21769/BioProtoc.3253.
55. Martinez Molina D, Jafari R, Ignatushchenko M, Seki T, Larsson EA, Dan C, Sreekumar L, Cao Y, and Nordlund P (2013). Monitoring drug target engagement in cells and tissues using the cellular thermal shift assay. Science 341, 84–87. 10.1126/science.1233606. [PubMed: 23828940]
56. Gerstein MB, Lu ZJ, Van Nostrand EL, Cheng C, Arshinoff BI, Liu T, Yip KY, Robilotto R, Rechtsteiner A, Ikegami K, et al. (2010). Integrative analysis of the *Caenorhabditis elegans* genome by the modENCODE project. Science 330, 1775–1787. 10.1126/science.1196914. [PubMed: 21177976]
57. Chandra V, Huang P, Potluri N, Wu D, Kim Y, and Rastinejad F (2013). Multidomain integration in the structure of the HNF-4alpha nuclear receptor complex. Nature 495, 394–398. 10.1038/nature11966. [PubMed: 23485969]
58. Cezairliyan B, Vinayavekhin N, Grenfell-Lee D, Yuen GJ, Saghatelian A, and Ausubel FM (2013). Identification of *Pseudomonas aeruginosa* phenazines that kill *Caenorhabditis elegans*. PLoS Pathog 9, e1003101. 10.1371/journal.ppat.1003101. [PubMed: 23300454]
59. Mahajan-Miklos S, Tan MW, Rahme LG, and Ausubel FM (1999). Molecular mechanisms of bacterial virulence elucidated using a *Pseudomonas aeruginosa-Caenorhabditis elegans* pathogenesis model. Cell 96, 47–56. [PubMed: 9989496]
60. Recinos DA, Sekedat MD, Hernandez A, Cohen TS, Sakhtah H, Prince AS, Price-Whelan A, and Dietrich LE (2012). Redundant phenazine operons in *Pseudomonas aeruginosa* exhibit environment-dependent expression and differential roles in pathogenicity. Proc Natl Acad Sci U S A 109, 19420–19425. 10.1073/pnas.1213901109. [PubMed: 23129634]
61. Tan MW, Mahajan-Miklos S, and Ausubel FM (1999). Killing of *Caenorhabditis elegans* by *Pseudomonas aeruginosa* used to model mammalian bacterial pathogenesis. Proc Natl Acad Sci USA 96, 715–720. [PubMed: 9892699]
62. Dirksen P, Marsh SA, Braker I, Heitland N, Wagner S, Nakad R, Mader S, Petersen C, Kowallik V, Rosenstiel P, et al. (2016). The native microbiome of the nematode *Caenorhabditis elegans*: gateway to a new host-microbiome model. BMC Biol 14, 38. 10.1186/s12915-016-0258-1. [PubMed: 27160191]
63. Samuel BS, Rowedder H, Braendle C, Felix MA, and Ruvkun G (2016). *Caenorhabditis elegans* responses to bacteria from its natural habitats. Proc Natl Acad Sci U S A 113, E3941–3949. 10.1073/pnas.1607183113. [PubMed: 27317746]

64. Simanek KA, Taylor IR, Richael EK, Lasek-Nesselquist E, Bassler BL, and Paczkowski JE (2022). The PqsE-RhlR Interaction Regulates RhlR DNA Binding to Control Virulence Factor Production in *Pseudomonas aeruginosa*. Microbiol Spectr 10, e0210821. 10.1128/spectrum.02108-21. [PubMed: 35019777]

65. Mukherjee S, Moustafa DA, Stergioula V, Smith CD, Goldberg JB, and Bassler BL (2018). The PqsE and RhlR proteins are an autoinducer synthase-receptor pair that control virulence and biofilm development in *Pseudomonas aeruginosa*. Proc Natl Acad Sci U S A 115, E9411–E9418. 10.1073/pnas.1814023115. [PubMed: 30224496]

66. Garcia-Reyes S, Cocotl-Yanez M, Soto-Aceves MP, Gonzalez-Valdez A, ServinGonzalez L, and Soberon-Chavez G (2021). PqsR-independent quorum-sensing response of *Pseudomonas aeruginosa* ATCC 9027 outlier-strain reveals new insights on the PqsE effect on RhlR activity. Mol Microbiol 116, 1113–1123. 10.1111/mmi.14797. [PubMed: 34418194]

67. Bent AF, and Mackey D (2007). Elicitors, effectors, and R genes: the new paradigm and a lifetime supply of questions. Annu Rev Phytopathol 45, 399–436. 10.1146/annurev.phyto.45.062806.094427. [PubMed: 17506648]

68. Jones JD, and Dangl JL (2006). The plant immune system. Nature 444, 323–329. 10.1038/nature05286. [PubMed: 17108957]

69. Pierson LS 3rd, and Pierson EA (2010). Metabolism and function of phenazines in bacteria: impacts on the behavior of bacteria in the environment and biotechnological processes. Appl Microbiol Biotechnol 86, 1659–1670. 10.1007/s00253-010-2509-3. [PubMed: 20352425]

70. Chin AWTF, Thomas-Oates JE, Lugtenberg BJ, and Bloemberg GV (2001). Introduction of the phzH gene of *Pseudomonas chlororaphis* PCL1391 extends the range of biocontrol ability of phenazine-1-carboxylic acid-producing *Pseudomonas* spp. strains. Mol Plant Microbe Interact 14, 1006–1015. 10.1094/MPMI.2001.14.8.1006. [PubMed: 11497461]

71. Mavrodi DV, Blankenfeldt W, and Thomashow LS (2006). Phenazine compounds in fluorescent *Pseudomonas* spp. biosynthesis and regulation. Annu Rev Phytopathol 44, 417–445. 10.1146/annurev.phyto.44.013106.145710. [PubMed: 16719720]

72. Dar D, Thomashow LS, Weller DM, and Newman DK (2020). Global landscape of phenazine biosynthesis and biodegradation reveals species-specific colonization patterns in agricultural soils and crop microbiomes. Elife 9. 10.7554/eLife.59726.

73. Lee DG, Urbach JM, Wu G, Liberati NT, Feinbaum RL, Miyata S, Diggins LT, He J, Saucier M, Deziel E, et al. (2006). Genomic analysis reveals that *Pseudomonas aeruginosa* virulence is combinatorial. Genome Biol 7, R90. 10.1186/gb-2006-7-10-r90. [PubMed: 17038190]

74. Shivers RP, Pagano DJ, Kooistra T, Richardson CE, Reddy KC, Whitney JK, Kamanzi O, Matsumoto K, Hisamoto N, and Kim DH (2010). Phosphorylation of the conserved transcription factor ATF-7 by PMK-1 p38 MAPK regulates innate immunity in *Caenorhabditis elegans*. PLoS Genet 6, e1000892. 10.1371/journal.pgen.1000892. [PubMed: 20369020]

75. Moura-Alves P, Fae K, Houthuys E, Dorhoi A, Kreuchwig A, Furkert J, Barison N, Diehl A, Munder A, Constant P, et al. (2014). AhR sensing of bacterial pigments regulates antibacterial defence. Nature 512, 387–392. 10.1038/nature13684. [PubMed: 25119038]

76. Moura-Alves P, Puyskens A, Stinn A, Klemm M, Guhlich-Bornhof U, Dorhoi A, Furkert J, Kreuchwig A, Protze J, Lozza L, et al. (2019). Host monitoring of quorum sensing during *Pseudomonas aeruginosa* infection. Science 366. 10.1126/science.aaw1629.

77. Brenner S (1974). The genetics of *Caenorhabditis elegans*. Genetics 77, 71–94. [PubMed: 4366476]

78. Fire A, Xu S, Montgomery MK, Kostas SA, Driver SE, and Mello CC (1998). Potent and specific genetic interference by double-stranded RNA in *Caenorhabditis elegans*. Nature 391, 806–811. 10.1038/35888. [PubMed: 9486653]

79. Rahme LG, Stevens EJ, Wolfort SF, Shao J, Tompkins RG, and Ausubel FM (1995). Common virulence factors for bacterial pathogenicity in plants and animals. Science 268, 1899–1902. [PubMed: 7604262]

80. Liberati NT, Urbach JM, Miyata S, Lee DG, Drenkard E, Wu G, Villanueva J, Wei T, and Ausubel FM (2006). An ordered, nonredundant library of *Pseudomonas aeruginosa* strain PA14 transposon

insertion mutants. Proc Natl Acad Sci U S A 103, 2833–2838. 10.1073/pnas.0511100103. [PubMed: 16477005]

81. Bolz DD, Tenor JL, and Aballay A (2010). A conserved PMK-1/p38 MAPK is required in *Caenorhabditis elegans* tissue-specific immune response to *Yersinia pestis* infection. J Biol Chem 285, 10832–10840. 10.1074/jbc.M109.091629. [PubMed: 20133945]
82. Yoneda T, Benedetti C, Urano F, Clark SG, Harding HP, and Ron D (2004). Compartment-specific perturbation of protein handling activates genes encoding mitochondrial chaperones. J Cell Sci 117, 4055–4066. 10.1242/jcs.01275. [PubMed: 15280428]
83. Qiu D, Damron FH, Mima T, Schweizer HP, and Yu HD (2008). PBAD-based shuttle vectors for functional analysis of toxic and highly regulated genes in *Pseudomonas* and *Burkholderia* spp. and other bacteria. Appl Environ Microbiol 74, 7422–7426. 10.1128/AEM.01369-08. [PubMed: 18849445]
84. Yunus AA, and Lima CD (2009). Purification of SUMO conjugating enzymes and kinetic analysis of substrate conjugation. Methods Mol Biol 497, 167–186. 10.1007/978-1-59745-566-4_11. [PubMed: 19107417]
85. Schindelin J, Arganda-Carreras I, Frise E, Kaynig V, Longair M, Pietzsch T, Preibisch S, Rueden C, Saalfeld S, Schmid B, et al. (2012). Fiji: an open-source platform for biological-image analysis. Nat Methods 9, 676–682. 10.1038/nmeth.2019. [PubMed: 22743772]
86. Han SK, Lee D, Lee H, Kim D, Son HG, Yang JS, Lee SV, and Kim S (2016). OASIS 2: online application for survival analysis 2 with features for the analysis of maximal lifespan and healthspan in aging research. Oncotarget 7, 56147–56152. 10.18632/oncotarget.11269. [PubMed: 27528229]
87. Bray NL, Pimentel H, Melsted P, and Pachter L (2016). Near-optimal probabilistic RNA-seq quantification. Nat Biotechnol 34, 525–527. 10.1038/nbt.3519. [PubMed: 27043002]
88. Pimentel H, Bray NL, Puente S, Melsted P, and Pachter L (2017). Differential analysis of RNA-seq incorporating quantification uncertainty. Nat Methods 14, 687–690. 10.1038/nmeth.4324. [PubMed: 28581496]
89. Subramanian A, Tamayo P, Mootha VK, Mukherjee S, Ebert BL, Gillette MA, Paulovich A, Pomeroy SL, Golub TR, Lander ES, and Mesirov JP (2005). Gene set enrichment analysis: a knowledge-based approach for interpreting genome-wide expression profiles. Proc Natl Acad Sci U S A 102, 15545–15550. 10.1073/pnas.0506580102. [PubMed: 16199517]
90. Holdorf AD, Higgins DP, Hart AC, Boag PR, Pazour GJ, Walhout AJM, and Walker AK (2020). WormCat: An Online Tool for Annotation and Visualization of *Caenorhabditis elegans* Genome-Scale Data. Genetics 214, 279–294. 10.1534/genetics.119.302919. [PubMed: 31810987]
91. Higgins DP, Weisman CM, Lui DS, D'Agostino FA, and Walker AK (2022). Defining characteristics and conservation of poorly annotated genes in *Caenorhabditis elegans* using WormCat 2.0. Genetics. 10.1093/genetics/iyac085.
92. Evans R, O'Neill M, Pritzel A, Antropova N, Senior A, Green T, Žídek A, Bates R, Blackwell S, Yim J, et al. (2022). Protein complex prediction with AlphaFold-Multimer. bioRxiv, 2021.2010.2004.463034. 10.1101/2021.10.04.463034.
93. Timmons L, Court DL, and Fire A (2001). Ingestion of bacterially expressed dsRNAs can produce specific and potent genetic interference in *Caenorhabditis elegans*. Gene 263, 103–112. 10.1016/s0378-1119(00)00579-5. [PubMed: 11223248]
94. Conte D Jr., MacNeil LT, Walhout AJM, and Mello CC (2015). RNA Interference in *Caenorhabditis elegans*. Curr Protoc Mol Biol 109, 26 23 21–26 23 30. 10.1002/0471142727.mb2603s109.
95. MacNeil LT, Pons C, Arda HE, Giese GE, Myers CL, and Walhout AJ (2015). Transcription Factor Activity Mapping of a Tissue-Specific in vivo Gene Regulatory Network. Cell Syst 1, 152–162. 10.1016/j.cels.2015.08.003. [PubMed: 26430702]
96. Kamath RS, Fraser AG, Dong Y, Poulin G, Durbin R, Gotta M, Kanapin A, Le Bot N, Moreno S, Sohrmann M, et al. (2003). Systematic functional analysis of the *Caenorhabditis elegans* genome using RNAi. Nature 421, 231–237. 10.1038/nature01278. [PubMed: 12529635]
97. Rual JF, Ceron J, Koreth J, Hao T, Nicot AS, Hirozane-Kishikawa T, Vandenhaute J, Orkin SH, Hill DE, van den Heuvel S, and Vidal M (2004). Toward improving *Caenorhabditis elegans*

phenome mapping with an ORFeome-based RNAi library. Genome Res 14, 2162–2168. 10.1101/gr.2505604. [PubMed: 15489339]

98. Dokshin GA, Ghanta KS, Piscopo KM, and Mello CC (2018). Robust Genome Editing with Short Single-Stranded and Long, Partially Single-Stranded DNA Donors in *Caenorhabditis elegans*. Genetics 210, 781–787. 10.1534/genetics.118.301532. [PubMed: 30213854]
99. Ghanta KS, and Mello CC (2020). Melting dsDNA Donor Molecules Greatly Improves Precision Genome Editing in *Caenorhabditis elegans*. Genetics 216, 643–650. 10.1534/genetics.120.303564. [PubMed: 32963112]
100. Labun K, Montague TG, Krause M, Torres Cleuren YN, Tjeldnes H, and Valen E (2019). CHOPCHOP v3: expanding the CRISPR web toolbox beyond genome editing. Nucleic Acids Res 47, W171–W174. 10.1093/nar/gkz365. [PubMed: 31106371]
101. Choi KH, Kumar A, and Schweizer HP (2006). A 10-min method for preparation of highly electrocompetent *Pseudomonas aeruginosa* cells: application for DNA fragment transfer between chromosomes and plasmid transformation. J Microbiol Methods 64, 391–397. 10.1016/j.mimet.2005.06.001. [PubMed: 15987659]
102. Visvikis O, Ihuegbu N, Labed SA, Luhachack LG, Alves AF, Wollenberg AC, Stuart LM, Stormo GD, and Irazoqui JE (2014). Innate host defense requires TFEB-mediated transcription of cytoprotective and antimicrobial genes. Immunity 40, 896–909. 10.1016/j.immuni.2014.05.002. [PubMed: 24882217]
103. Wong D, Bazopoulou D, Pujol N, Tavernarakis N, and Ewbank JJ (2007). Genome-wide investigation reveals pathogen-specific and shared signatures in the response of *Caenorhabditis elegans* to infection. Genome Biol 8, R194. 10.1186/gb-2007-8-9-r194. [PubMed: 17875205]
104. Somasiri P, Behm CA, Adamski M, Wen J, and Verma NK (2020). Transcriptional response of *Caenorhabditis elegans* when exposed to *Shigella flexneri*. Genomics 112, 774–781. 10.1016/j.ygeno.2019.05.016. [PubMed: 31125598]
105. Pfaffl MW (2001). A new mathematical model for relative quantification in real-time RT-PCR. Nucleic Acids Res 29, e45. [PubMed: 11328886]
106. Dowen RH (2019). CEH-60/PBX and UNC-62/MEIS Coordinate a Metabolic Switch that Supports Reproduction in *C. elegans*. Dev Cell 49, 235–250 e237. 10.1016/j.devcel.2019.03.002. [PubMed: 30956009]
107. Gao JL, Kwan AH, Yammine A, Zhou X, Trewhella J, Hugrass BM, Collins DAT, Horne J, Ye P, Harty D, et al. (2018). Structural properties of a haemophore facilitate targeted elimination of the pathogen Porphyromonas gingivalis. Nat Commun 9, 4097. 10.1038/s41467-018-06470-0. [PubMed: 30291238]
108. Foster KJ, McEwan DL, and Pukkila-Worley R (2020). Measurements of Innate Immune Function in *C. elegans*. Methods Mol Biol 2144, 145–160. 10.1007/978-1-0716-0592-9_13. [PubMed: 32410032]
109. Schiessl KT, Hu F, Jo J, Nazia SZ, Wang B, Price-Whelan A, Min W, and Dietrich LEP (2019). Phenazine production promotes antibiotic tolerance and metabolic heterogeneity in *Pseudomonas aeruginosa* biofilms. Nat Commun 10, 762. 10.1038/s41467-019-08733-w. [PubMed: 30770834]
110. Jorgensen WL, Maxwell DS, and Tirado-Rives J (1996). Development and testing of the OPLS all-atom force field on conformational energetics and properties of organic liquids. Journal of the American Chemical Society 118, 11225–11236.
111. Halgren T (2007). New method for fast and accurate binding-site identification and analysis. Chem Biol Drug Des 69, 146–148. 10.1111/j.1747-0285.2007.00483.x. [PubMed: 17381729]
112. Friesner RA, Banks JL, Murphy RB, Halgren TA, Klicic JJ, Mainz DT, Repasky MP, Knoll EH, Shelley M, Perry JK, et al. (2004). Glide: a new approach for rapid, accurate docking and scoring. 1. Method and assessment of docking accuracy. J Med Chem 47, 1739–1749. 10.1021/jm0306430. [PubMed: 15027865]
113. Harder E, Damm W, Maple J, Wu C, Reboul M, Xiang JY, Wang L, Lupyan D, Dahlgren MK, Knight JL, et al. (2016). OPLS3: A Force Field Providing Broad Coverage of Drug-like Small Molecules and Proteins. J Chem Theory Comput 12, 281–296. 10.1021/acs.jctc.5b00864. [PubMed: 26584231]

## Highlights

- PCN, a metabolite secreted by *P. aeruginosa*, activates innate immunity in *C. elegans*
- The *C. elegans* nuclear hormone receptor NHR-86 is the sensor for PCN
- PCN binds to NHR-86 and activates its anti-pathogen transcriptional program
- PCN is surveilled by *C. elegans* to assess the relative threat of virulent *P. aeruginosa*

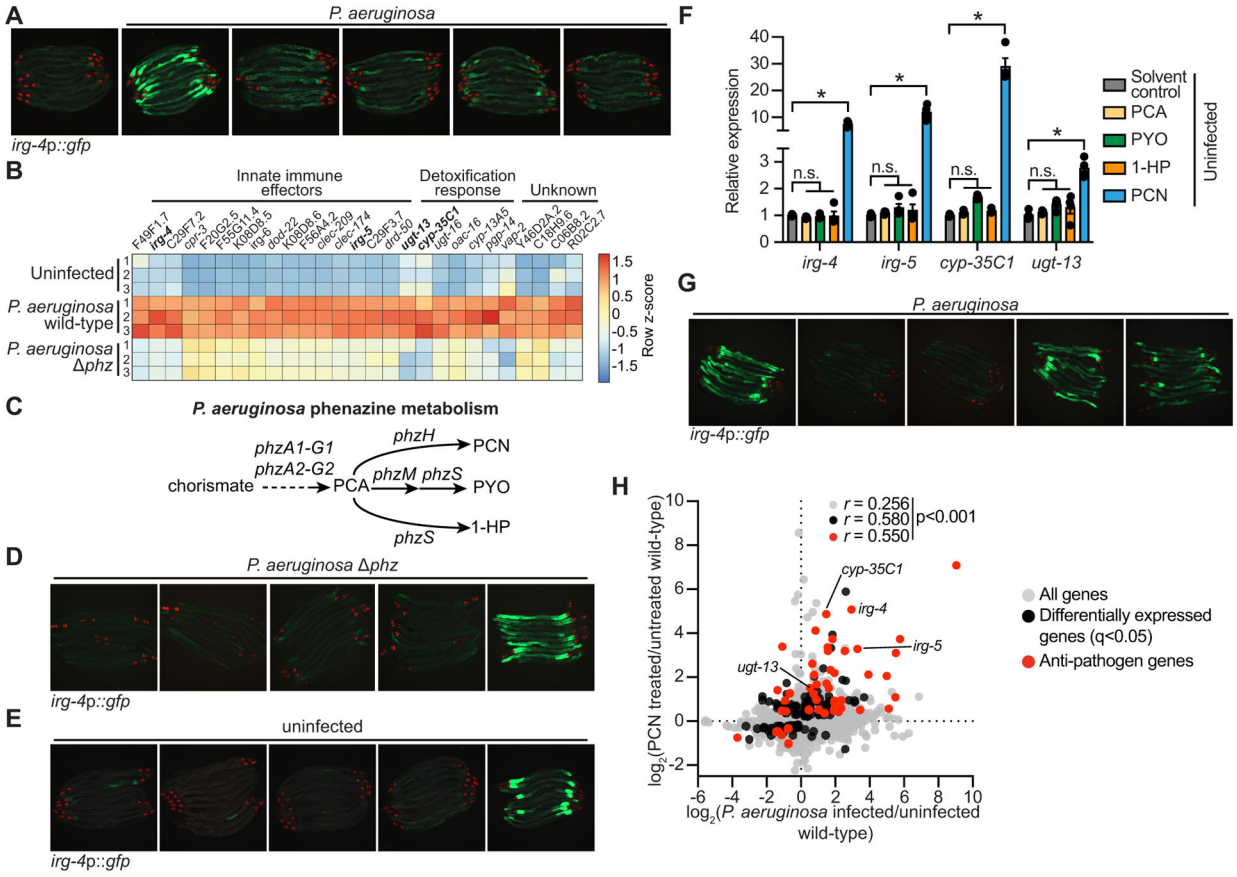


**Figure 1. The pathogen-derived metabolite phenazine-1-carboxamide (PCN) activates anti-pathogen defenses in the *C. elegans* intestine.**

**(A)** Images of *C. elegans irg-4*p::*gfp* transcriptional reporter expression in animals either uninfected or infected with the indicated *P. aeruginosa* strains, (scale bar, 200 μM). **(B)** Heat map of the 27 genes that are induced in *C. elegans* during *P. aeruginosa* infection in a manner dependent on the production of phenazines (q<0.05). Gene expression from biological replicates in each condition were scaled by calculating the row z-score for each gene ($n$=3). See also Table S1A. **(C)** A schematic of *P. aeruginosa* phenazine metabolism (PCA, phenazine-1-carboxylic acid; PCN, phenazine-1-carboxamide; PYO, pyocyanin; 1-HP, 1-hydroxyphenazine). **(D and E)** Images of *C. elegans irg-4*p::*gfp* animals during infection with *P. aeruginosa* Δ*phz* **(D)** or grown under standard conditions (uninfected) **(E)** on media that was supplemented with the indicated phenazines, (scale bar, 200 μM). **(F)** qRT-PCR analysis of the indicated anti-pathogen genes in wild-type animals exposed to the indicated phenazines in the absence of infection. Data are the average of biological replicates with error bars giving SEM ($n$=4). *equals p<0.05 (Brown-Forsythe and Welch ANOVA with Dunnett's T3 multiple comparisons test). Concentration of phenazines used in (D), (E) and (F) are 112 μM PCN, 112 μM PCA, 119 μM PYO, and 25 μM 1-HP. **(G)** Images of *C. elegans irg-4*p::*gfp* animals infected with the indicated *P. aeruginosa* strains. (scale bar, 200 μM). **(H)** Data from mRNA-sequencing experiments comparing genes differentially regulated in wild-type animals exposed to PCN (y-axis) with genes differentially expressed in wild-type animals during *P. aeruginosa* infection (x-axis). All

genes are shown in gray. Genes that are differentially expressed in both datasets are shown in black ($q<0.05$), and the differentially expressed genes annotated as anti-pathogen genes (innate immune effector or detoxification genes) are shown in red. The Pearson correlation coefficient ($r$) between the indicated transcriptional signatures is shown. The location of the genes *irg-4*, *irg-5*, *cyp-35C1*, and *ugt-13*, whose regulation is examined throughout this manuscript, are shown. See also Table S1B. Source data for this figure is in Table S3. See also Fig. S1.

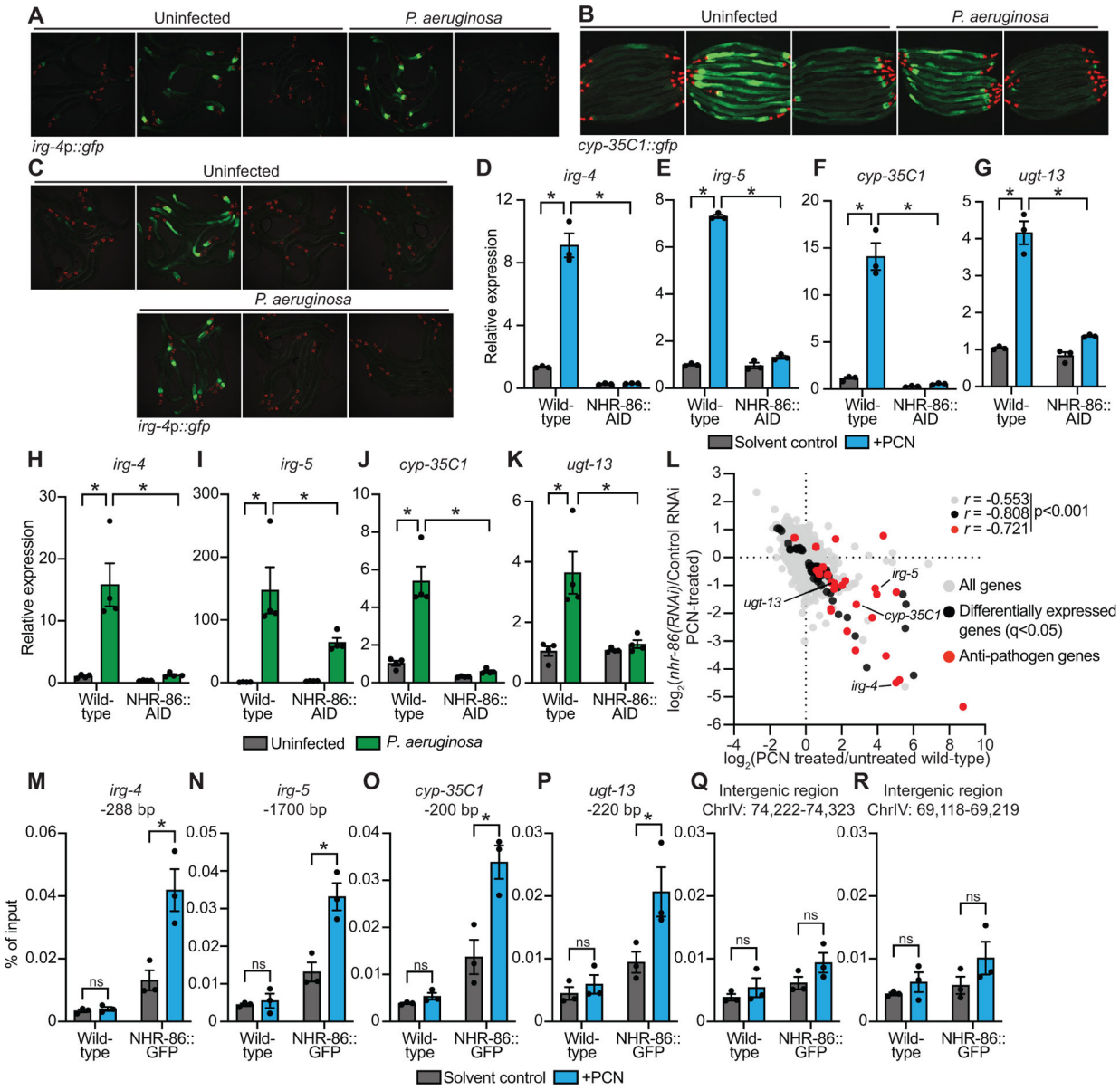


**Figure 2. The anti-pathogen transcriptional program induced by PCN requires the *C. elegans* nuclear hormone receptor *nhr-86*.**

**(A and B)** Images of *C. elegans irg-4*p::*gfp* **(A)** and *cyp-35C1*::*gfp* **(B)** transcriptional reporters with indicated RNAi conditions either exposed to PCN in the absence of infection or during *P. aeruginosa* infection, (scale bar, 200 μM). **(C)** Images of *C. elegans irg-4*p::*gfp* transcriptional reporters with indicated genotypes and conditions, (scale bar, 200 μM). **(D-K)** qRT-PCR analysis of the indicated innate immune genes in wild-type and NHR-86::AID animals exposed to either PCN in the absence of infection ($n$=3) **(D-G)** or during infection with *P. aeruginosa* ($n$=4) **(H-K)**. All conditions are in the presence of auxin. Data are the mean of biological replicates with error bars giving SEM. *equals p<0.05 (two-way ANOVA with Tukey's multiple comparisons test) **(L)** Data from mRNA-sequencing experiments comparing genes differentially regulated in *nhr-86(RNAi)* versus control RNAi-treated

animals exposed to PCN (y-axis) are compared with genes differentially expressed in wild-type animals exposed to PCN (x-axis). All genes are shown in gray. Genes that are differentially expressed in both datasets are shown in black (q<0.05), and the differentially expressed genes annotated as anti-pathogen genes (innate immune effector or detoxification genes) are shown in red. The Pearson correlation coefficient (*r*) between the indicated transcriptional signatures is shown. The location of the genes *irg-4*, *irg-5*, *cyp-35C1*, and *ugt-13*, whose regulation is examined throughout this manuscript, are shown. (*n*=3) See also Table S1C. **(M-R)** ChIP-qPCR analysis of NHR-86 binding to the indicated DNA regions in wild-type and NHR-86::GFP animals exposed to solvent control or PCN. Protein-DNA complexes were immunoprecipitated with a α-GFP antibody. Data are the mean of biological replicates with error bars giving SEM (*n*=3). *equals p<0.05 (two-way ANOVA with Tukey's multiple comparisons test). Source data for this figure is in Table S3. See also Fig. S2.

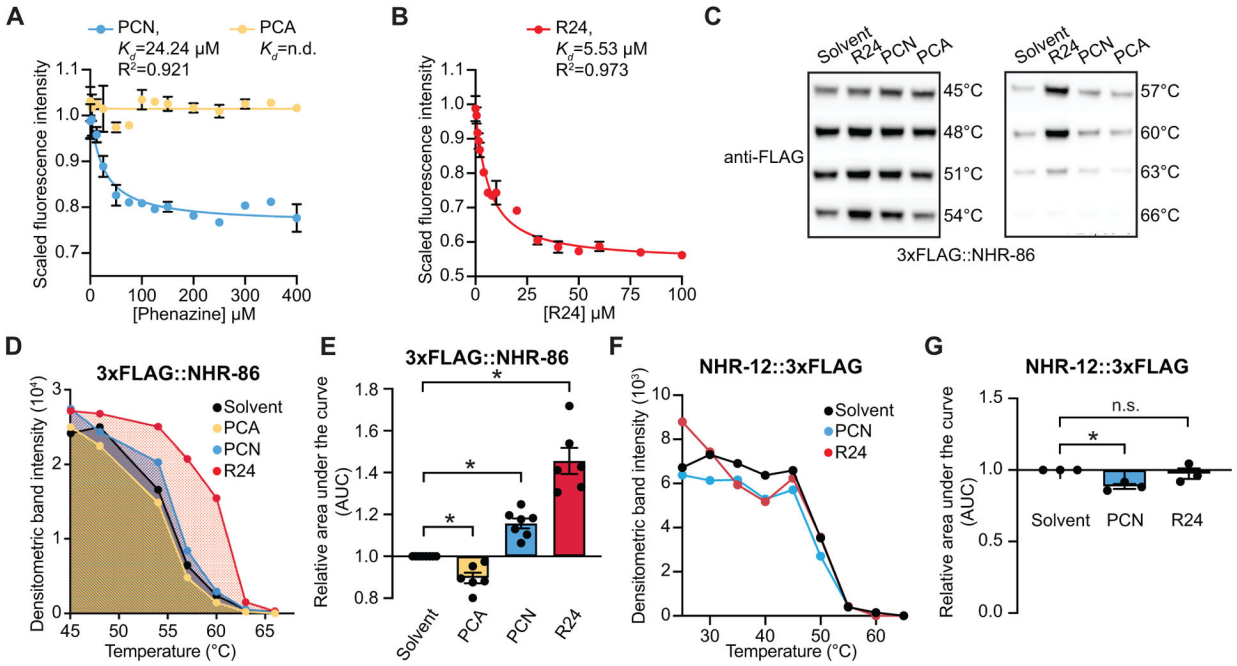


**Figure 3. The bacterial metabolite PCN and synthetic immunostimulatory molecule R24 bind to the ligand-binding domain of NHR-86.**

**(A and B)** Intrinsic tryptophan fluorescence intensity of the purified ligand-binding domain (LBD) of NHR-86 treated with the indicated concentrations of PCN **(A)**, PCA **(A),** and R24 **(B)**, each normalized to the solvent control-treated samples. Curves represent a non-linear regression fit of the scaled fluorescence intensity data points for each condition. An equilibrium dissociation constant ($K_d$) and goodness of fit calculation ($R^2$) are shown for each curve. Data in (A) and (B) are the average of biological replicate samples ($n$=3) with error bars giving SEM. SDS-PAGE analysis of purified NHR(LBD) is shown in Fig. S3A. **(C)** A representative immunoblot of a cellular thermal shift assay (CETSA) experiment using an anti-FLAG antibody that probed whole cell lysates from a transgenic *C. elegans* strain in which NHR-86 was tagged with 3xFLAG at its endogenous locus. **(D)** A representative densitometric quantification from a CETSA experiment that characterized the interaction of PCN (400–500 µM) ($n$=7), PCA (400–500 µM) ($n$=6), and R24 (70 µM) ($n$=6) with 3xFLAG::NHR-86. **(E)** The area under the curve was quantified from each biological replicate experiment for the experiment described in (D) and normalized to the solvent control condition. All biological replicates for this experiment are shown in Fig. S3B. **(F)** Quantification of NHR-12::3xFLAG immunoblot band intensities for each treatment condition and temperature from a representative experiment. **(G)** The area under the curve was quantified from each biological replicate for the experiment described in (F) and normalized to the solvent control condition ($n$=3). All biological replicates for this experiment are shown in Fig. S3C. Data in (E) and (G) are the average of all biological replicates with error bars giving SEM. *equals $p<0.05$ (two-tailed, unpaired t-test with Welch's correction). The structures of R24, PCN and PCA are show in Fig. S3D. Source data for this figure is in Table S3. See also Fig. S3.

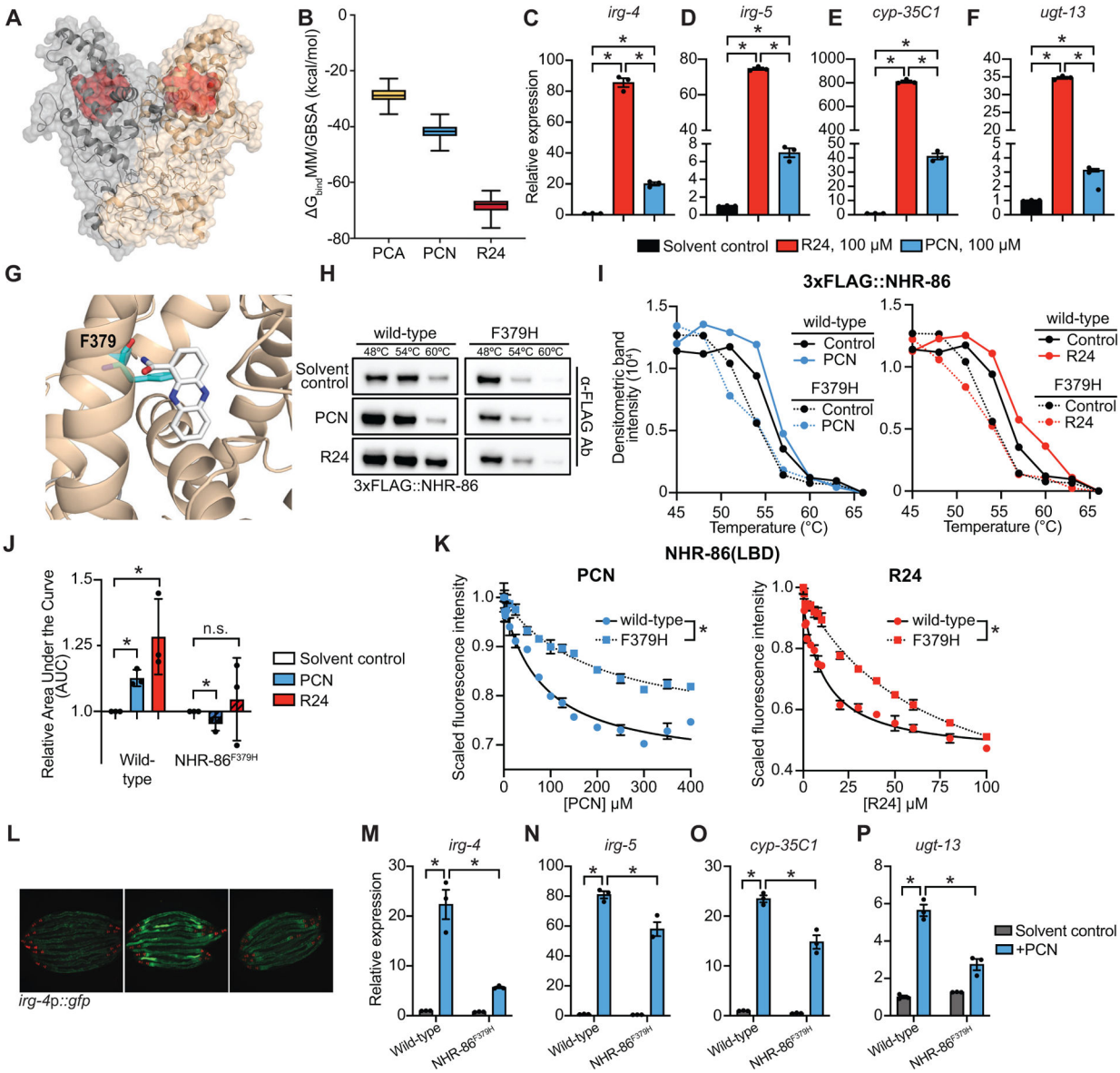


**Figure 4. The phenylalanine at position 379 of NHR-86 is required for binding of PCN and R24.**

**(A)** *In silico* molecular modeling of full-length apo NHR-86 as a homodimer. The identified ligand-binding pocket is indicated in red. **(B)** Average free energy of ligand-binding for PCA, PCN, and R24 calculated using the molecular mechanics/generalized Born surface area (MM/GBSA). See also Supplemental Video S1. **(C-F)** qRT-PCR analysis of wild-type animals exposed to either solvent control (1% DMSO) or 100 µM R24 or 100 µM PCN. Data are the average of biological replicates ($n$=3) with error bars giving SEM. *equals $p<0.05$ (Brown-Forsythe and Welch ANOVA with Dunnett's multiple comparisons test). **(G)** An *in silico* model of PCN bound to the identified binding pocket in the NHR-86(LBD). The interaction of phenylalanine 379 (F379) (cyan) and PCN (white) is shown. **(H)** A representative immunoblot of a CETSA experiment using an anti-FLAG antibody that probed whole cell lysates from *C. elegans* 3xFLAG::NHR-86 and 3xFLAG::NHR-86$^{F379H}$ strains treated with indicated conditions. **(I)** A representative densitometric quantification

from a CETSA experiment that characterized the interaction of solvent control, PCN, and R24 with 3xFLAG::NHR-86 and 3xFLAG::NHR-86$^{F379H}$ ($n$=3) **(J)** The area under the curve was quantified from each biological replicate for the experiment described in (I) and normalized to the solvent control condition of 3xFLAG::NHR-86 (n=3). All biological replicates for this experiment are shown in Fig. S4B. Data are the average of all biological replicates with error bars giving SEM. *equals p<0.05 (two-tailed, unpaired t-test with Welch's correction). **(K)** Intrinsic tryptophan fluorescence intensity of the purified ligand-binding domain (LBD) of wild-type NHR-86 and NHR-86 containing the F379H mutation treated with the indicated concentrations of PCN and R24 each normalized to the solvent control-treated samples. Curves represent a non-linear regression fit of the scaled fluorescence intensity data points for each condition. Data are the average of biological replicate samples ($n$=3) with error bars giving SEM. *equals p<0.05 (unpaired t-test with Welch's correction) for equilibrium dissociation constant ($K_d$) between the wild-type NHR-86(LBD) and the NHR-86$^{F379H}$ mutant protein. SDS-PAGE analysis of purified NHR(LBD)$^{F379H}$ is shown in Fig. S3A. **(L)** Images of indicated *C. elegans irg-4*p::*gfp* animals grown on media that was supplemented with PCN (448 μM) or solvent control, as indicated, (scale bar, 200 μM). **(M-P)** qRT-PCR analysis of the indicated innate immune genes in wild-type and NHR-86$^{F379H}$ animals exposed to either solvent control or PCN (448 μM) in the absence of infection. Data are the mean of biological replicates ($n$=3) with error bars giving SEM. *equals p<0.05 (two-way ANOVA with Tukey's multiple comparisons test). Source data for this figure is in Table S3. See also Fig. S4.

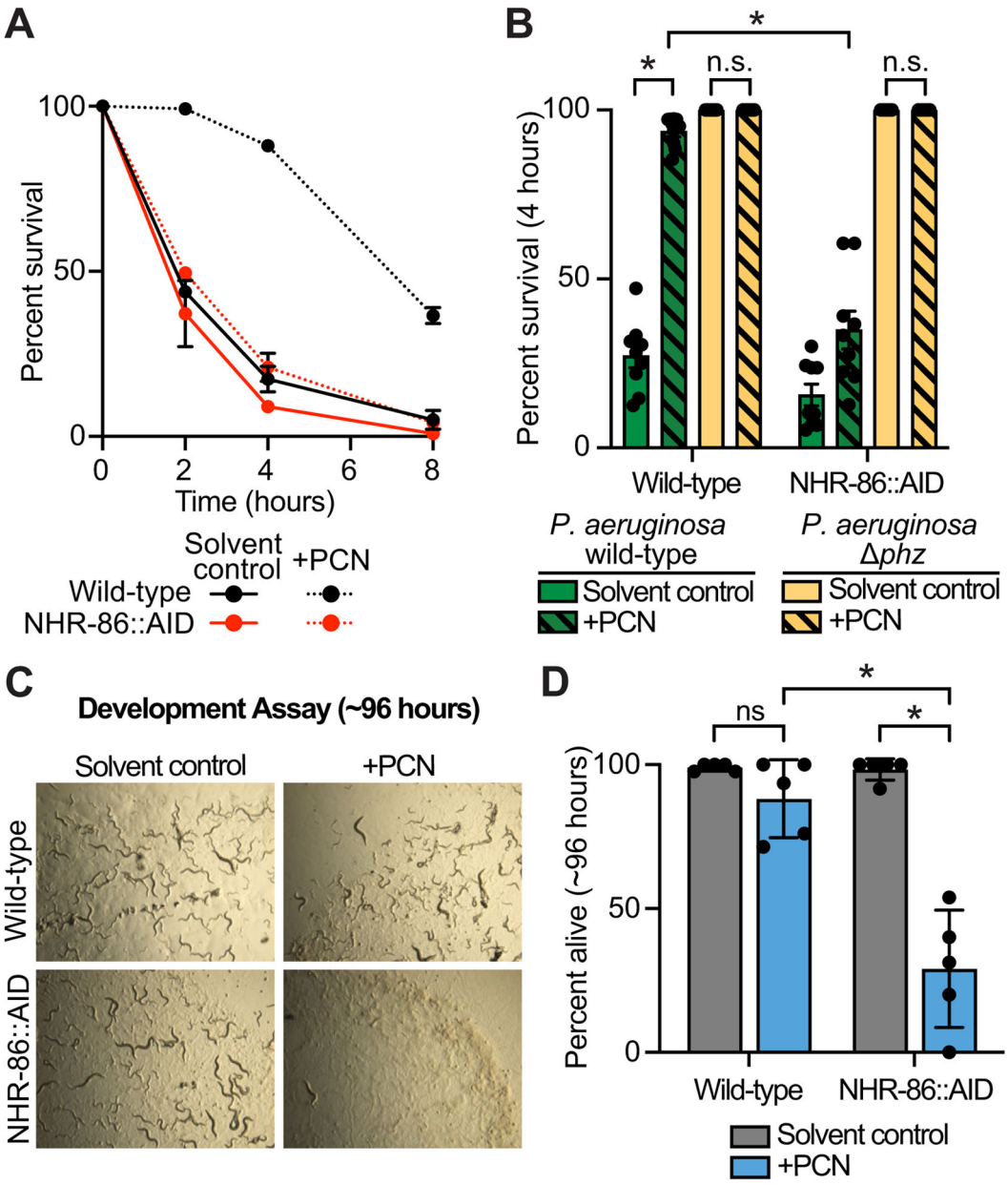


**Figure 5. The bacterial metabolite PCN is a pattern of pathogenesis sensed by *C. elegans* NHR-86 to activate innate immunity.**

**(A)** A phenazine toxicity assay in *C. elegans* (also called the "fast kill" assay) with *P. aeruginosa* and *C. elegans* of the indicted genotypes either treated with solvent control or PCN (448 μM). Data are representative of three trials. The difference between PCN-treated wild-type and NHR-86::AID animals is significant ($p<0.05$, log-rank test, $n=3$). Survival curves for these strains exposed to the *P. aeruginosa* Δ*phz* mutant are shown in Fig. S5A. Sample sizes, four-hour survival, and p-values for each replicate are shown in Table S2.

**(B)** Survival data at four hours after exposure to the indicated conditions is shown for the experiment described in (A). Data are the average of three biological replicates each containing three trials with error bars showing SEM ($n=9$). *equals $p<0.05$ (two-way ANOVA with Tukey's multiple comparisons test). Sample sizes, four-hour survival, and

p-values for each replicate are shown in Table S2. **(C and D)** A development assay with wild-type and NHR-86::AID *C. elegans*. Animals of the indicated genotypes were allowed to lay their brood in the presence or absence of PCN, as indicated, and **(C)** photographed after approximately 96 hours or **(D)** scored for the number of alive animals ($n$=5). All assay plates contained 50 μM auxin. *p<0.05 for the indicated comparisons (two-way ANOVA with Šídák's multiple comparisons test). n.s.=not significant. Source data for this figure is in Table S3. See also Fig. S5.

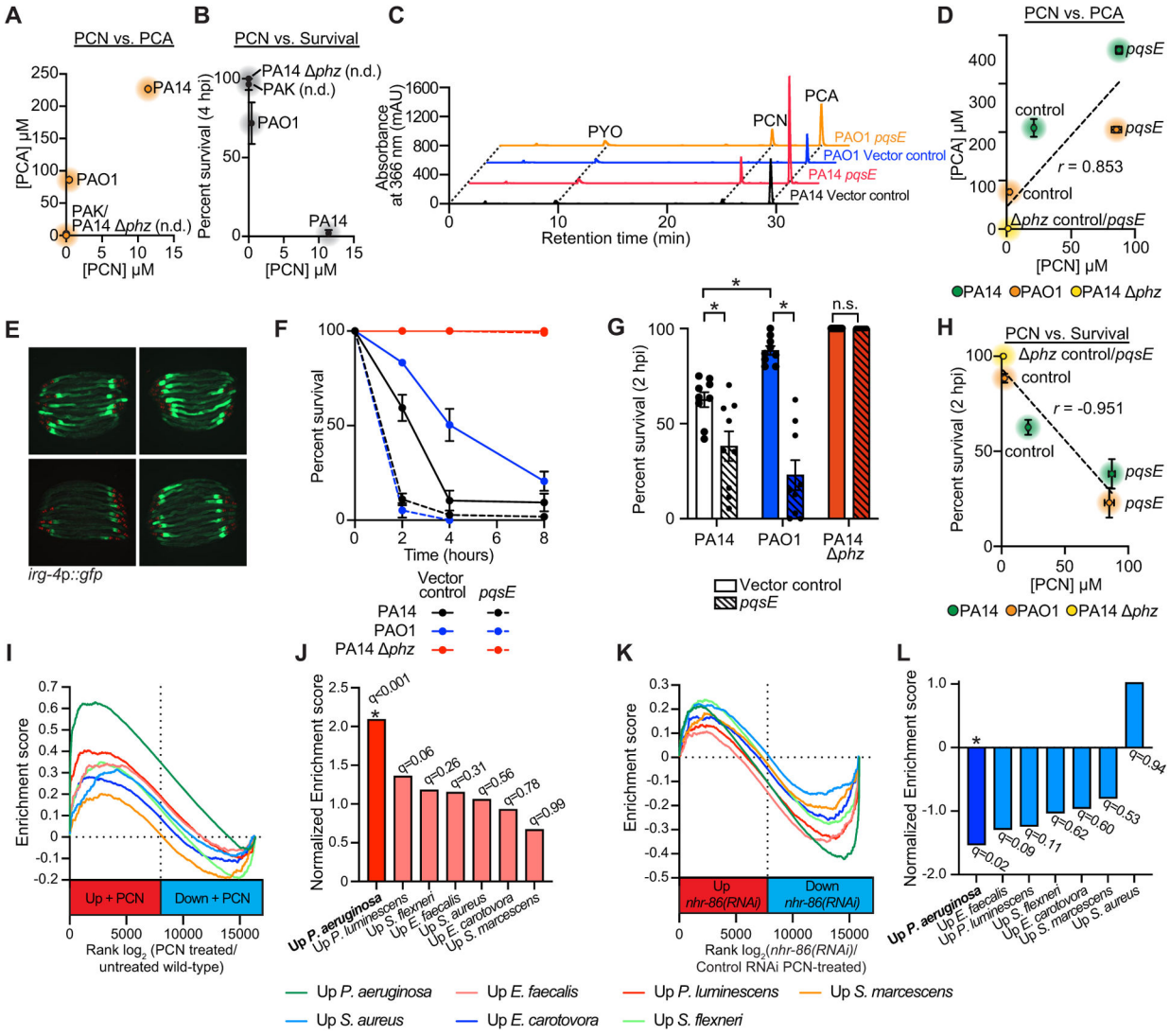


**Figure 6. *C. elegans* sense PCN to assess the relative threat of virulent *P. aeruginosa*, but not other pathogenic bacteria.**

**(A-C)** HPLC-UV spectroscopy was used to quantify the individual phenazines in the indicated *P. aeruginosa* strains. **(A)** PCN production was compared to PCA production in biological replicates of the indicated *P. aeruginosa* strains ($n$=3). See Fig. S6 for the comparison of PCN production with 1-HP (Fig. S6A) and PYO (Fig. S6B) in these strains. **(B)** PCN production was compared to the pathogenicity of *P. aeruginosa* towards *C. elegans* in the phenazine toxicity assay, as quantified by percent nematode survival at four hours. n.d.=PCN was not detected. **(C)** Liquid chromatography-UV chromatograms of *P. aeruginosa* PA14 or PAO1 strains that express *pqsE* in multicopy (*pqsE*) or a control plasmid (vector control). See Fig. S6 for a comparison of PCA (Fig. S6D) and PCN (Fig. S6E) production in these strains. **(D)** HPLC-UV spectroscopy data showing the comparison of PCN production versus PCA production in biological replicates of the indicated *P. aeruginosa* strains. Pearson correlation coefficient ($r$) is significant ($p<0.05$, $n$=3). **(E)** Images of *C. elegans irg-4*p::*gfp* animals infected with the indicated *P. aeruginosa*

strains, (scale bar, 200 μM). **(F)** Phenazine toxicity assay with wild-type *C. elegans* and indicated *P. aeruginosa* strains. The difference between the PAO1 control vector and *pqsE* overexpression is significant ($p<0.05$, log-rank test, $n=3$). Data is representative of three biological replicates. **(G)** Survival data at two hours for strains of the indicated genotypes is shown for the experiment described (F). Data are the average of three biologicals replicates each containing three trials with error bars showing SEM ($n=9$). *equals $p<0.05$ (two-way ANOVA with Tukey's multiple comparisons test). Sample sizes, two-hour survival, and p-values for each replicate are shown in Table S2. **(H)** Comparison of PCN production in the indicated *P. aeruginosa* genotypes with their pathogenicity toward *C. elegans* in the phenazine toxicity assay is presented. Pearson correlation coefficient ($r$) from biological replicates is significant ($p<0.05$, $n=3$). See also Table S3 for the HPLC-UV and LC-MS/MS phenazine retention times and abundance for the data shown in (A-D) and (H). **(I)** Gene set enrichment analysis (GSEA) examining the genes that are differentially regulated in wild-type *C. elegans* exposed to PCN, as determined by mRNA-seq (See Fig. 1H). Fold change in expression of genes in uninfected animals exposed to PCN are presented in rank order on the x-axis from higher expression (red) to lower expression (blue) and compared to the genes that are induced upon exposure to the indicated pathogens. **(J)** GSEA normalized enrichment score (NES) and q-value for the comparisons shown in (I). Only the comparison of genes whose transcription changes in the presence of PCN and during *P. aeruginosa* infection was significant ($q<0.05$). **(K)** A similar GSEA as described in (I) except genes whose transcription depend on *nhr-86* during PCN treatment (See Fig. 2L) are compared to genes induced upon exposure to the indicated pathogens. **(L)** GSEA normalized enrichment score (NES) and q-value for the experiment described in (K) are shown. As in (J), only the comparison with genes induced during *P. aeruginosa* infection was significant ($q<0.05$). Source data for this figure is in Table S3. See also Fig. S6.

## KEY RESOURCES TABLE

| REAGENT or RESOURCE | SOURCE | IDENTIFIER |
|---|---|---|
| **Antibodies** | | |
| Anti-FLAG M2, Mouse, Monoclonal, Unconjugated | Sigma-Aldrich | Cat# F1804; RRID:AB_262044 |
| Anti-alpha-Tubulin, Mouse, Monoclonal, Unconjugated | Sigma-Aldrich | Cat# T5168; RRID:AB_477579 |
| Anti-Actin, Rabbit, Recombinant, Unconjugated | Abcam | Cat# ab179467 RRID:AB_2737344 |
| Anti-phospho-p38 MAPK (Thr180/Tyr182), Rabbit | Cell Signaling Technology | Cat # 9211S; RRID:AB_331641 |
| Anti-total-p38 MAPK, Rabbit | Peterson et al.[39] | N/A |
| Goat Anti-Rabbit IgG, HRP-linked | Cell Signaling Technology | Cat# 7074; RRID:AB_2099233 |
| Goat Anti-Mouse IgG - H&L, Polyclonal, HRP Conjugated | Abcam | Cat# ab6789; RRID:AB_955439 |
| Anti-GFP, Mouse, Monoclonal, Unconjugated (clones 7.1 and 13.1) | Sigma-Aldrich | Cat# 11814460001; RRID:AB_390913 |
| **Bacterial and virus strains** | | |
| *Escherichia coli* OP50 | Brenner[77] | WB Cat# WBStrain00041969; RRID:WB-STRAIN:WBStrain00041969 |
| *E. coli* HT115(DE3) | Fire et al.[78] | WB Cat# WBStrain00041080; RRID:WB-STRAIN:WBStrain00041080 |
| *E. coli* DH5α | New England BioLabs | Cat# C2987H |
| *E. coli* BL21(DE3) | New England BioLabs | Cat# C2527H |
| *Pseudomonas aeruginosa* (UCBPP-PA14) | Rahme et al.[79] | RRID:WB-STRAIN: WBStrain00041978 |
| *P. aeruginosa* (PAK) | Lee et al.[73] | N/A |
| *P. aeruginosa* (PAO1) | Lee et al.[73] | N/A |
| *P. aeruginosa* PA14 Δ*phzA1-G1* Δ*phzA2-G2* (Δphz) | Dietrich et al.[49] | N/A |
| *P. aeruginosa* PA14 Δ*gacA* | Troemel et al.[7] | N/A |
| *P. aeruginosa* PA14 Δ*rhlR* | Rahme et al.[79] | N/A |
| *P. aeruginosa* PA14 Δ*lasR* | Fred Ausubel | N/A |
| *P. aeruginosa* PA14 Δ*pqsR* | Fred Ausubel | N/A |
| *P. aeruginosa* PA14 transposon mutants | Liberati et al.[80] | N/A |
| *P. aeruginosa* PAO1 *(pqsE* overexpression) | This study | N/A |
| *P. aeruginosa* PA14 *(pqsE* overexpression) | This study | N/A |
| **Chemicals, peptides, and recombinant proteins** | | |
| 5-Fluoro-2'-deoxyuridine | Sigma-Aldrich | Cat# CAF0503 |
| (−) Tetramisole hydrochloride | Sigma-Aldrich | Cat# L9756–10G |
| Q5 High-Fidelity DNA Polymerase | New England BioLabs | Cat# R0101 |
| Isopropyl-β-D-thiogalactoside (IPTG) | GoldBio | Cat# I2481C200 |
| Trizol | Thermo Fisher Scientific | Cat# 15596018 |
| Proteinase K | New England BioLabs | Cat# P8107S |
| Ethylenediaminetetraacetic acid (EDTA), 0.5M, pH 8.0 | Thermo Fisher Scientific | Cat# 1860851 |

| REAGENT or RESOURCE | SOURCE | IDENTIFIER |
|---|---|---|
| HALT Protease Inhibitor Cocktail (100X) | Thermo Fisher Scientific | Cat# 78430 |
| Phenol:chloroform:isoamyl alcohol | Thermo Fisher Scientific | Cat# 15593031 |
| Phenazine-1-carboxylic acid | Ark Pharm | Cat# AK-98673 |
| Phenazine-1-carboxamide | Princeton BioMolecular Research | Cat# PBMR030086 |
| 1-hydroxyphenazine | TCI America | Cat# H0289 |
| Pyocyanin | Cayman Chemicals | Cat# 10009594 |
| Auxin α-napthaleneacetic acid (K-NAA) | PhytoTech Labs | Cat# N610 |
| SpCas9 Nuclease | IDT | Cat# 1081058 |
| A.s. Cas12a (Cpf1) Ultra | IDT | Cat# 10001273 |
| Ulp1 protease | Thermo Fisher Scientific | Cat# SAE0067 |
| Ni-NTA resin | Qiagen | Cat# 30210 |
| Imidazole | Sigma-Aldrich | Cat# I5513 |
| N-acetyl-L-trytophanamide (NATA) | Sigma-Aldrich | Cat# A6501 |
| Methanol for HPLC | Thermo Fisher Scientific | Cat# 61009–0040 |
| 16% Formaldehyde Solution (w/v) | Thermo Fisher Scientific | Cat# 28908 |
| Gentamycin sulfate | Sigma | Cat# G1264 |
| Streptomycin sulfate | Thermo Fisher Scientific | Cat# AC612240500 |
| **Critical commercial assays** | | |
| iScript gDNA Clear cDNA Synthesis Kit | Bio-Rad | Cat# 172–5034 |
| *DC* Protein Assay | Bio-Rad | Cat# 5000111 |
| iTaq Universal SYBR Green Supermix | Bio-Rad | Cat# 172–5120 |
| Q5 Site-Directed Mutagenesis Kit | New England BioLabs | Cat# E0552S |
| NEBuilder HiFi DNA Assembly master mix | New England BioLabs | Cat# E2621 |
| **Deposited data** | | |
| Raw and analyzed mRNA-Seq data | This study | GSE202258 |
| **Experimental models: Organisms/Strains** | | |
| *C. elegans*: Strain: N2 (Bristol) | Brenner[77] | WB Cat# WBStrain00000001; RRID:WB-STRAIN:WBStrain00000001 |
| *C. elegans*: Strain: AU307 *agIs44[irg-4p::gfp::unc-54–3'UTR;myo-2p::mCherry]* | Pukkila-Worley et al.[41] | N/A |
| *C. elegans*: Strain: AY101 *acIs101 [pDB09.1(irg-5p::gfp)*; pRF4(rol-6(su1006))] | Bolz et al.[81] | WB Cat# WBStrain00000322; RRID: WB-STRAIN:WBStrain00 000322 |
| *C. elegans*: Strain: VL491 *nhr-86(tm2590)* | Arda et al.[50] | WB Cat# WBStrain00040127; RRID: WB-STRAIN:WBStrain00 040127 |
| *C. elegans*: Strain: RPW137 *nhr-86(ums12)* | Peterson et al.[39] | N/A |
| *C. elegans*: Strain: RPW99 *nhr-86(tm2590);agIs44 [irg-4p::gfp::unc-54–3'UTR;myo-2p::mCherry]* | Peterson et al.[39] | N/A |
| *C. elegans*: Strain: RPW106 *nhr-86(tm2590);acIs101 [pDB09.1(irg-5p::gfp); pRF4(rol-6(su1006))]* | Peterson et al.[39] | N/A |
| *C. elegans*: Strain: RPW165 *nhr-86(ums12); agIs44 [irg-4p::gfp::unc-54–3 ' UTR;myo-2p::mCherry]* | Peterson et al.[39] | N/A |

| REAGENT or RESOURCE | SOURCE | IDENTIFIER |
|---|---|---|
| *C. elegans*: Strain: SJ4100 *zcIs13 [hsp-6::gfp + lin-15(+)]* | Yoneda et al.[82] | WB Cat # WBStrain00034068; RRID:WB-STRAIN:WBStrain00034068 |
| *C. elegans*: Strain: CA1200 *ieSi57 [eft-3p::TIR1::mRuby::un54 3'UTR + Cbr-unc-119(+)]* | Zhang et al.[51] | WB Cat # WBStrain00004055; RRID:WB-STRAIN:WBStrain00004055 |
| *C. elegans*: Strain: OP318 *unc-119(ed3); wgIs318* [*nhr-12::TY1::EGFP::3xFLAG(92C12)+unc-119(+)]* | Gerstein et al.[56] | WB Cat # WBStrain00030124; RRID:WB-STRAIN:WBStrain00030124 |
| *C. elegans*: Strain: RPW423 *umsEx88[cyp-35C1p::gfp::unc-54–3'* UTR; *myo-2p::mCherry]* | This study | N/A |
| *C. elegans*: Strain: RPW348 *nhr-86(ums64[NHR-86::AID])*; ieSi57 *[eft-3p::TIR1::mRuby::un54* 3'UTR + *Cbr-unc-119(+)]* | This study | N/A |
| *C. elegans*: Strain: RPW424 *nhr-86(ums65[3xFLAG::NHR-86])*; ieSi57 *[eft-3p::TIR1::mRuby::un54* 3'UTR + *Cbr-unc-119(+)]* | This study | N/A |
| *C. elegans*: Strain: RPW427 *nhr-86(ums66[3xFLAG::NHR-86::AID])*; ieSi57 *[eft-3p::TIR1::mRuby::un54 3'*UTR + *Cbr-unc-119(+)]* | This study | N/A |
| *C. elegans*: Strain: RPW191 *nhr-86(ums14[3xFLAG::NHR-86])* | This study | N/A |
| *C. elegans*: Strain: RPW401 *nhr-86(ums14[3xFLAG::NHR-86]); agIs44 [irg-4p::gfp::unc-54–3 VTR;myo-2p::mCherry]* | This study | N/A |
| *C. elegans*: Strain: RPW430 *nhr-86(ums67[3xFLAG::NHR-86[F379H]]);agIs44 [irg-4p::gfp::unc-54-* 3' *\UTR;myo-2p::mCherry]* | This study | N/A |
| *C. elegans*: Strain: MGH167 *sid-1(qt9); aIxIs9* [vha-6p::s/d-1::SL2::GFP] | Melo et al.[19] | N/A |
| **Experimental models: Media** | | |
| Bacto peptone | Thermo Fisher Scientific | Cat# 211677 |
| BD Bacto agar | BD | Cat# 214030 |
| **Oligonucleotides** | | |
| See Table S4 | This study | N/A |
| **Recombinant DNA** | | |
| pHERD30T | Qiu et al.[83] | NovoPro Cat# V005565 |
| pSMT3 | Yunus et al.[84] | N/A |
| pPD95.75 | Addgene plasmid # 1494 | RRID:Addgene_1494 |
| pHER30T::pqsE | This study | N/A |
| pSMT3::nhr-86 ligand binding domain | This study | N/A |
| pSMT3::nhr-86$^{F379H}$ ligand binding domain | This study | N/A |
| *pPD95.75::cyp-35C1p::gfp* | This study | N/A |
| **Software and algorithms** | | |
| Fiji/ImageJ | Schindelin et al.[85] | RRID:SCR_002285 |
| OASIS 2 | Han et al.[86] | RRID:SCR_014450 |
| R Console (Version 3.5) | The R Foundation | RRID:SCR_001905 |

| REAGENT or RESOURCE | SOURCE | IDENTIFIER |
|---|---|---|
| FastQC (Version 0.11.5) | https://www.bioinformatics.babraham.ac.uk/projects/fastqc/ | RRID:SCR_014583 |
| Kallisto (version 0.45.0) | Bray et al.[87] | RRID:SCR_016582 |
| Sleuth (version 0.30.0) | Pimentel et al.[88] | RRID:SCR_002555 |
| GSEA (version 4.1.0) | Subramanian et al.[89] | RRID:SCR_003199 |
| pheatmap (version 1.0.12) | https://cran.r-project.org/web/packages/pheatmap/index.html | RRID:SCR_016418 |
| WormCat 2.0 | Holdorf et al.[90]; Higgins et al.[91] | N/A |
| GraphPad Prism 9 | https://www.graphpad.com/scientific-software/prism/ | RRID:SCR_002798 |
| AlphaFold-Multimer | Evans et al.[92] | N/A |
| Schrodinger v.19–4 | https://www.schrodinger.com | RRID:SCR_014879 |
| **Other** | | |
| 0.22 μm cellulose Spin-X columns | Thermo Fisher Scientific | Cat# 07–200-386 |
| HPLC screw-top vials with fixed inserts | Agilent Technologies | Cat# 5188–6592 |
| Biphenyl HPLC column (4.6 × 150 mm, 2.6 μm) | Kinetex | Cat# 00F-4622-E0 |
| Dynabead Protein G | Invitrogen | Cat# 10004D |